

1 **Spatial and seasonal variability in volatile organic sulfur**  
2 **compounds in seawater and the overlying atmosphere of the**  
3 **Bohai and Yellow Seas**

4 **Juan Yu<sup>1,2,3,†</sup>, Lei Yu<sup>1,†</sup>, Zhen He<sup>1,2,3</sup>, Gui-Peng Yang<sup>1,2,3,\*</sup>, Jing-Guang Lai<sup>1</sup>, Qian Liu<sup>1</sup>**

5 <sup>1</sup>Frontiers Science Center for Deep Ocean Multispheres and Earth System, Key Laboratory of Marine Chemistry  
6 Theory and Technology, Ministry of Education, Ocean University of China, Qingdao 266100, China.

7 <sup>2</sup>Laboratory for Marine Ecology and Environmental Science, Qingdao National Laboratory for Marine Science and  
8 Technology, Qingdao 266237, China.

9 <sup>3</sup>Institute of Marine Chemistry, Ocean University of China, Qingdao 266100, China.

10  
11 **Abstract.** Volatile organic sulfur compounds (VSCs), including carbon disulfide (CS<sub>2</sub>), dimethyl sulfide (DMS), and  
12 carbonyl sulfide (COS), were surveyed in the seawater of the Bohai and Yellow Seas and the overlying atmosphere  
13 during spring and summer of 2018 to understand the production and loss of VSCs and their influence factors. The  
14 concentration ranges of COS, DMS, and CS<sub>2</sub> in the surface seawater were 0.14–0.42, 0.41–7.74, and 0.01–0.18 nmol  
15 L<sup>-1</sup> during spring and 0.32–0.61, 1.31–18.12, and 0.01–0.65 nmol L<sup>-1</sup> during summer, respectively. The COS  
16 concentrations exhibited positive correlation with dissolved organic carbon (DOC) concentrations in seawater during  
17 summer, which verified the photochemical production of COS from chromophoric dissolved organic matter (CDOM).  
18 High DMS concentrations occurred near the Yellow River, Laizhou Bay, and Yangtze River Estuary, coinciding with  
19 high nitrate and Chl *a* concentrations due to river discharge during summer. The COS, DMS, and CS<sub>2</sub> concentrations  
20 were the highest in the surface seawater and decreased with the depth. The mixing ratios of COS, DMS, and CS<sub>2</sub> in

---

\* Corresponding author at: Key Laboratory of Marine Chemistry Theory and Technology, Ministry of Education, Ocean University of China, 238 Songling Road, Qingdao 266100, China. E-mail address: gpyang@mail.ouc.edu.cn (G.-P. Yang)

†These authors contributed equally to this work and should be considered co-first authors.

21 the atmosphere were 255.9–620.2 pptv, 1.3–191.2 pptv, and 5.2–698.8 pptv during spring and 394.6–850.1 pptv,  
22 10.3–464.3 pptv, and 15.3–672.7 pptv in summer, respectively. The ratios of mean oceanic concentrations and  
23 atmospheric mixing ratios for summer to spring in COS, DMS, and CS<sub>2</sub> were 1.8, 3.1, 3.7 and 1.6, 4.6, 1.5, respectively.  
24 The ratios of the mean sea-to-air fluxes for summer to spring in COS, DMS, and CS<sub>2</sub> were 1.2, 2.1, and 4.3. The sea-  
25 to-air fluxes of VSCs indicated that the marginal seas are important sources of VSCs in the atmosphere. The results  
26 provide help with a better understanding of the contribution of VSCs in marginal seas.

27 **Keywords:** Volatile organic sulfur compound; Carbonyl sulfide; Dimethyl sulfide; Carbon disulfide

## 28 **1 Introduction**

29 Carbonyl sulfide (COS), dimethyl sulfide (DMS), and carbon disulfide (CS<sub>2</sub>) are three major volatile organic sulfur  
30 compounds (VSCs) in seawater and the marine atmosphere. Their biogeochemical cycles are closely related to climate  
31 change (Charlson et al., 1987; Li et al., 2022). VSCs contribute to the formation of atmospheric cloud condensation  
32 nuclei (CCN) and sulfate aerosols, significantly affecting the global radiation budget and ozone concentration  
33 (Andreae and Crutzen, 1997). Hence, interest in the distribution, production, and chemistry of VSCs has grown in  
34 recent years (Lennartz et al., 2017; Lennartz et al., 2020; Li et al., 2022; Remaud et al., 2022; Whelan et al., 2018;  
35 Yang et al., 2008; Yu et al., 2022). Production and loss processes of COS, DMS, and CS<sub>2</sub> have been documented by  
36 many researchers in the following manners.

37 COS has an average tropospheric residence time of 2–7 years and is the most abundant and widely distributed  
38 reduced sulfur trace gas in the atmosphere (Brühl et al., 2012). COS can be converted to sulfate aerosols in the  
39 stratosphere, affecting the Earth's radiation balance (Crutzen, 1976). Atmospheric COS originates directly from  
40 oceanic emissions and indirectly from the oxidation of DMS and CS<sub>2</sub> (Kettle et al., 2002; Lennartz et al., 2020).  
41 Uptake by terrestrial vegetation and soil is the most important sink of atmospheric COS (Kettle et al., 2002; Maignan  
42 et al., 2021). Therefore, COS can be used as a proxy for estimating the photosynthesis rate in ecosystems (Campbell  
43 et al., 2008). COS production is dependent on UV radiation, chromophoric dissolved organic matter (CDOM), cysteine,  
44 and nitrate concentration (Lennartz et al., 2021; Li et al., 2022). Some studies have indicated that the ocean is a COS  
45 source (Chin and Davis, 1993; Yu et al., 2022), whereas others have shown that the ocean is a COS sink (Zhu et al.,  
46 2019).

47 Atmospheric DMS can react with OH and NO<sub>3</sub> radicals to form SO<sub>2</sub> and methane sulfonic acid (MSA, CH<sub>3</sub>SO<sub>3</sub>H),  
48 creating non-sea salt sulfates (nss-SO<sub>4</sub><sup>2-</sup>), which contribute to acid deposition and CCN (Charlson et al., 1987). DMS  
49 is the predominant biogenic sulfur originating from dimethylsulfoniopropionate (DMSP), predominantly produced by  
50 bacteria and phytoplankton (Curson et al., 2017; Keller et al., 1989). DMSP lyase from phytoplankton and bacteria  
51 can convert DMSP to DMS (Reisch et al., 2011). The community composition of phytoplankton and bacteria can  
52 affect the net DMSP concentrations via synthesis and degradation (O'Brien et al., 2022, Zhao et al., 2021). DMS

53 entering the atmosphere via sea-to-air exchange accounts for about 50% of all natural sulfur releases (Cline and Bates,  
54 1983).

55 CS<sub>2</sub> is the key precursor of COS, and 82% COS is the oxidation production of CS<sub>2</sub> (Lennartz et al., 2020).  
56 Photochemical reaction with dissolved organic matter (DOM) is a principal source of CS<sub>2</sub> in seawater (Xie et al.,  
57 1998). The photochemical reaction of DOM generates excited triplet states of chromophoric dissolved organic matter  
58 (<sup>3</sup>CDOM\*), singlet oxygen (<sup>1</sup>O<sub>2</sub>), hydrogen peroxide (H<sub>2</sub>O<sub>2</sub>), and hydroxyl radical (·OH). These reactive species  
59 subsequently interact with DMS, resulting in the production of CS<sub>2</sub> (Modiri Gharehveran and Shah, 2021). The  
60 oxidation reaction involving the OH radicals and CS<sub>2</sub> is a substantial contributor to the generation of SO<sub>2</sub>, which  
61 subsequently leads to the production of acid rain (Logan et al., 1979). Anthropogenic CS<sub>2</sub> sources include rayon and/or  
62 aluminum production, fuel combustion, oil refineries, and coal combustion (Campbell et al., 2015; Zumkehr et al.,  
63 2018).

64 Two different approaches (ice core and isotope measurements) were used to evaluate anthropogenic COS emissions  
65 (Aydin et al., 2020; Hattori et al., 2020). The latter study and a modeling approach used by Remaud et al. (2022)  
66 observed a gradient of anthropogenic COS in East Asia. Anthropogenic COS is initially emitted as CS<sub>2</sub> and oxidized  
67 by OH to COS in the atmosphere (Kettle et al., 2002). The production and loss of DMS involve phytoplankton and  
68 bacteria synthesis, zooplankton grazing, bacterial degradation, and sea-air diffusion (Schäfer et al., 2010). COS and  
69 CS<sub>2</sub> production are related to photo-oxidation and/or photochemical reactions (Lennartz et al., 2020; Xie et al., 1998).  
70 However, the production and loss mechanisms remain unclear.

71 The Yellow Sea (YS) and Bohai Sea (BS) are semi-enclosed seas in the northwestern Pacific Ocean. The BS coastal  
72 current, YS coastal current, and YS warm current substantially affect the hydrological characteristics of this area  
73 (Chen, 2009), potentially altering the VSC distributions via water mass exchanges. In addition, the Yellow Sea Cold  
74 Water Mass (YSCWM), a seasonal hydrological phenomenon located in the 35°N transect, forms, peaks, and  
75 disappears in spring, summer, and after September, respectively (Zhang et al., 2014). In this study, we investigate the  
76 spatial distributions and seasonal variability of COS, DMS, and CS<sub>2</sub> in the seawater and overlying atmosphere of the

77 YS and BS and the effects of the YSCWM (the 35°N transect) on the VSC distributions to better understand the  
78 distributions and impact factors of VSCs in Chinese marginal seas.

## 79 **2 Materials and methods**

### 80 **2.1 Sampling**

81 Two cruises were conducted aboard the R/V “Dong Fang Hong 2” in the YS and BS from 27 March to 16 April  
82 (spring) 2018 and from 24 July to 8 August (summer) 2018. The sampling stations are shown in Fig. 1. Surface and  
83 depth seawater samples were collected using 12 L Niskin bottles mounted on a Seabird 911 conductivity-temperature-  
84 depth (CTD) rosette. Surface seawater was sampled at a depth of 3–5 m. The seawater was slowly siphoned from the  
85 Niskin bottles into 100 mL glass jaw bottles (CNW Technologies GmbH, GER) via a translucent silicone tube. The  
86 seawater was allowed to overflow the sampling bottle by twice its volume before the silicone tube was gently removed,  
87 and the bottle was immediately sealed with an aluminum cap containing a Teflon-lined butyl rubber septum without  
88 any headspace. Subsequently, the concentrations of oceanic VSCs were immediately measured on the ship. The  
89 environmental and hydrological parameters such as seawater temperature and salinity were measured simultaneously  
90 by the CTD equipment.

91 Atmospheric VSC samples were collected using cleaned and vacuumed SilcoCan canisters (Restek, USA) in the  
92 windward direction approximately 10 m above the ocean. The stability of VSCs in fused silica-lined canisters has  
93 been verified during storage for 16 d at room temperature (Brown et al., 2015). The atmospheric samples were  
94 analyzed immediately after being brought back to the laboratory.

### 95 **2.2 Analytical procedures**

96 The VSC concentrations in the seawater were measured using a gas chromatograph (GC) (Agilent 7890A, USA) with  
97 a flame photometric detector (FPD). The atmospheric VSC mixing ratios were measured using a GC equipped with a  
98 mass spectrometer (GC-MS) (Agilent 7890A/5975C, USA) using the methods of Inomata et al. (2006) and Staubes  
99 and Georgii (1993), respectively. A CP-Sil 5 CB column (30 m × 0.32 mm × 4.0 μm, Agilent Technologies, USA)  
100 was used to separate the three VSCs. Standard VSC gases with mixing ratios of 1 ppmv were bought from Beijing  
101 Minnick Analytical Instrument Equipment Center. Qualitative analysis was conducted by comparing the results with

102 the retention times of the standards, and quantitative analysis was conducted by diluting the VSC standard gases to 1  
103 ppbv and 5 ppbv using a 2202A dynamic dilution meter (Nutech, USA) and injecting different volumes of the diluted  
104 VSC standards into the GC using a gas-tight syringe. The VSC mixing ratios were calculated after calibration using  
105 standard gases (Fig. S1).

106 The VSC concentrations in seawater were determined using a cryogenic purge-and-trap system coupled with the  
107 GC-FPD. A 30 mL seawater sample was injected into a glass bubbling chamber with a gas-tight syringe (SGE,  
108 Australia). The VSCs were extracted from the seawater with high purity N<sub>2</sub> at a rate of 60 mL min<sup>-1</sup> for 15 min and  
109 passed through an anhydrous CaCl<sub>2</sub>-filled drying tube and a 100% degreased cotton-filled 1/4 Teflon tube to remove  
110 water and oxides. Subsequently, the VSC gases were passed through a six-way valve and trapped in a loop of the 1/16  
111 Teflon capture tube immersed in liquid nitrogen. After all VSCs had been purged from the seawater, the capture tube  
112 was removed from the liquid nitrogen and placed into hot water (> 90 °C) to desorb the trapped VSCs. The VSCs gases  
113 were carried into the GC by N<sub>2</sub> and detected by the FPD. The column temperature was programmed with an initial  
114 temperature of 55 °C, followed by an increase to 100 °C at 10 °C min<sup>-1</sup> and a final increase to 150 °C at 15 °C min<sup>-1</sup>.  
115 The inlet and detector temperatures were 150 °C and 160 °C, respectively, and the split ratio of pure N<sub>2</sub> was 10:1. The  
116 detection limits of the method for COS, DMS, and CS<sub>2</sub> were 33 pg, 387 pg, and 22 pg and the measurement precision  
117 was 5.59%–11.70% (Tian et al., 2005). The DMS concentrations in seawater were obtained from Zhang et al. (2023).

118 The mixing ratios of atmospheric VSCs were analyzed using an Entech 7100 pre-concentrator (Nutech, USA)  
119 coupled with GC-MS. The sample SilcoCan canister was connected to the pre-concentrator, and 200 mL of gas was  
120 drawn into the preconcentration system with a three-stage cold trap (Fig. S1). The pre-concentrator parameters of the  
121 three-stage cold trap are listed in Table S1. The first trap removes N<sub>2</sub>, O<sub>2</sub>, and H<sub>2</sub>O (g) from the atmospheric samples,  
122 and the second trap eliminates CO<sub>2</sub>. The third trap is used to separate the three VSCs and obtain better peak shapes.  
123 The temperature programming of the column was the same as for the seawater samples. In addition, the temperature  
124 of the quadrupole and ion source were 110 °C and 230 °C, respectively, and the electron ionization source was run at  
125 70 eV. The carrier gas had a split ratio of 10:1 and a flow rate of 2.0 mL min<sup>-1</sup>. Qualitative and quantitative analyses  
126 of the VSCs were conducted using the full scan mode (SCAN) and the selected ion monitoring mode (SIM). The  
127 mass-to-charge ratios (*m/z*) for COS, DMS, and CS<sub>2</sub> were 60, 62, and 76, respectively. The detection limit of the VSCs

128 was 0.1–0.5 pptv (Zhu et al., 2017).

### 129 **2.3 Calculation of sea-to-air fluxes of VSCs**

130 The sea-to-air fluxes of the VSCs were calculated using the model established by Liss and Slater (1974):  $F = k_w(c_w -$   
131  $c_g/H)$ , where  $F$  is the sea-to-air flux of VSCs ( $\mu\text{mol m}^{-2} \text{d}^{-1}$ );  $k_w$  is the VSC transfer velocity ( $\text{m d}^{-1}$ );  $c_w$  and  $c_g$  are the  
132 equilibrium concentrations of VSCs in the surface seawater and the atmosphere ( $\text{nmol L}^{-1}$ ), respectively; and  $H$  is  
133 Henry's constant calculated using the equation listed in Table S2 (De Bruyn et al., 1995; Dacey et al., 1984). It was  
134 converted to a dimensionless constant using the equation proposed by Sander (2015).  $k_w$  was calculated from the wind  
135 speed, and the sea surface temperature was obtained by the N2000 method (Nightingale et al., 2000). The  $C_g$  of DMS  
136 is assumed to be zero in this study. This is based on the fact that atmospheric mixing ratios of DMS are typically  
137 several orders of magnitude lower than concentrations in seawater (Turner et al., 1996). We used the calculation  
138 developed by Kettle et al. (2001).

### 139 **2.4 Measurements of Chl *a*, nutrients, and dissolved organic carbon**

140 The seawater samples for the analysis of the Chl *a* concentrations were filtered through Whatman GF/F filters, and  
141 the filtrate was stored in darkness at  $-20^\circ\text{C}$ . Then, Chl *a* was extracted with 90% acetone for 24 h at  $4^\circ\text{C}$  in darkness.  
142 The Chl *a* concentrations were determined following the method of Parsons et al. (1984) with a fluorescence  
143 spectrophotometer (F-4500, Hitachi) at excitation/emission wavelengths of 436 nm/670 nm. The seawater was filtered  
144 through Whatman GF/F filters ( $0.7 \mu\text{m}$ ), and the filtered water samples were stored at  $-20^\circ\text{C}$  before nutrient (nitrate,  
145 phosphate, and silicate) analysis. A Technicon Autoanalyser AAII (SEAL Analytical, UK) was used to measure the  
146 nitrate, phosphate, and silicate concentrations. The nitrate, phosphate, and silicate data were provided by the open  
147 research cruise supported by the National Natural Science Foundation (NSFC) Shiptime Sharing Project.

148 The dissolved organic carbon (DOC) concentrations were measured using the method of Chen et al. (2021). The  
149 seawater was filtered through Whatman GF/F filters (pre-combusted at  $500^\circ\text{C}$  for 4 h), and the filtrate was stored at  
150  $-20^\circ\text{C}$  for DOC analysis. The DOC concentrations were determined by a total organic carbon analyzer (Shimadzu  
151 TOC-VCPH) after adding two drops of 12 mol/L HCl.

### 152 **2.5 Data analysis**

153 SPSS 24.0 software (SPSS Inc., Chicago, IL, USA) was used to analyze the relationships between the environmental  
154 factors and the concentrations and mixing ratios of the three VSCs in seawater and the atmosphere during spring and  
155 summer.

## 156 **3 Results**

### 157 **3.1 Spatial distributions of COS, DMS, and CS<sub>2</sub> in surface seawater**

#### 158 **3.1.1 Spring distributions**

159 The temperature in the surface seawater showed a decreasing trend from south to north, and the salinity increased  
160 from the inshore to the offshore sites due to the influences of the YS warm current, Yalu River, and Yellow River  
161 (Fig. 2). The Chl *a* concentrations in the surface water of the BS and YS in the spring were 0.17–4.45  $\mu\text{g L}^{-1}$  with an  
162 average of  $1.19 \pm 0.96 \mu\text{g L}^{-1}$ . The highest Chl *a* concentration occurred at station B39 in the BS (Fig. 2), which may  
163 be related to the enhanced phytoplankton growth due to the abundance of nutrients resulting from a seawater exchange  
164 between the BS and YS. In addition, high Chl *a* concentrations were observed in the central area of the southern YS.

165 The concentrations of COS, DMS, and CS<sub>2</sub> in the surface seawater of the BS and YS during spring were 0.14–0.42,  
166 0.41–7.74, and 0.01–0.18  $\text{nmol L}^{-1}$ , with mean values of  $0.24 \pm 0.06$ ,  $1.74 \pm 1.61$ , and  $0.07 \pm 0.05 \text{ nmol L}^{-1}$ ,  
167 respectively (Fig. 2). The high COS concentrations during the spring occurred in the YS (Fig. 2). The highest COS  
168 concentration was observed at station H21, coinciding with a high Chl *a* concentration. The two areas with high  
169 concentrations of COS in the central waters of the southern YS overlapped with areas with high Chl *a* concentrations.  
170 High DMS concentrations existed in the coastal waters of the southern Shandong Peninsula, as well as at station B21  
171 in the central part of the northern YS. The distribution of CS<sub>2</sub> in seawater exhibited a decreasing trend from inshore  
172 to offshore (Fig. 2). High CS<sub>2</sub> concentrations appeared at stations H18 and H19 in the coastal waters of YSCWM (Fig.  
173 2). There was also a high CS<sub>2</sub> concentration at station B30 near the shore of the Liaodong Peninsula (Fig. 2).

#### 174 **3.1.2 Summer distributions**

175 The temperature and salinity in the BS and YS in summer were relatively high, and high Chl *a* concentrations were  
176 concentrated in coastal waters (Fig. 3). The Chl *a* concentrations in the seawater during summer were 0.10–4.74  $\mu\text{g}$   
177  $\text{L}^{-1}$  with an average of  $1.60 \pm 1.19 \mu\text{g L}^{-1}$ . Station B43 near the Yellow River estuary and Laizhou Bay had the highest



178 Chl *a* concentration, which may have been due to the abundance of nutrients (nitrate: 5.85  $\mu\text{mol L}^{-1}$ , silicate: 17  $\mu\text{mol}$   
179  $\text{L}^{-1}$ ) carried by nearby rivers or coastal currents (Figs. 3 and S2). Low salinities and high nitrate and Chl *a*  
180 concentrations occurred at Stations H32, H34, and H35 in the northeast of the Yangtze River Estuary and at Stations  
181 B66 and B68 near the Laizhou Bay and Yellow River Estuary (Figs. 3 and S2).

182 The concentrations of COS, DMS, and CS<sub>2</sub> in the surface water of the BS and YS during summer were 0.32–0.61,  
183 1.31–18.12, and 0.01–0.65  $\text{nmol L}^{-1}$ , with mean values of  $0.44 \pm 0.06$ ,  $5.43 \pm 3.60$ , and  $0.26 \pm 0.15$   $\text{nmol L}^{-1}$ ,  
184 respectively (Fig. 3). The ratios of the mean concentrations between summer and spring for Chl *a*, COS, DMS, and  
185 CS<sub>2</sub> were 1.3, 1.8, 3.1, and 3.7, respectively. High COS concentrations were observed at stations B38 and B54 in the  
186 BS during summer. In addition, COS had a high concentration at station H25 in the central part of the southern YS,  
187 close to a location with a high CS<sub>2</sub> concentration (Fig. 3). High DMS concentrations were common in the northern BS  
188 and were generally coincident with high Chl *a* levels. However, high Chl *a* and DMS concentrations were found in  
189 the coastal waters of the Yangtze River Estuary due to the Changjiang diluted water. In addition, the DMS  
190 concentration was high at station H12 (Fig. 3). There were high CS<sub>2</sub> concentrations in the northeastern area of the  
191 Yangtze River estuary (Fig. 3).

## 192 **3.2 Depth distributions of COS, DMS, and CS<sub>2</sub> in seawater**

### 193 **3.2.1 Depth distributions in spring**

194 The temperature and Chl *a* decreased from the surface to the bottom seawater (Fig. 4). The ratios of the mean  
195 concentrations between the surface and greater depths (> 60 m) were 5.4, 5.1, 5.9, and 8.9 for Chl *a*, COS, DMS, and  
196 CS<sub>2</sub>, respectively (Fig. 4). Consistent with the Chl *a* distribution, the depth distribution of DMS in the seawater  
197 decreased from the euphotic zone to the bottom seawater (Fig. 4). High COS concentrations occurred in the surface  
198 seawater and decreased with the depth, and the lowest concentrations occurred in the bottom waters. CS<sub>2</sub> exhibited  
199 depth gradients at most stations during spring, with higher concentrations at the surface, except for station H15 where  
200 the CS<sub>2</sub> concentrations were high in the bottom seawater.

### 201 **3.2.2 Depth distributions in summer**

202 The YSCWM affected the depth distributions in summer in the 35°N transect. Substantial temperature differences

203 occurred between the surface and bottom seawater in summer, and stratification in the water bodies was observed (Fig.  
204 5). A distinct thermocline existed at a depth of 20 m, indicating the formation of the YSCWM (Fig. 5). All high Chl  
205 *a* concentrations in the surveyed area of the BS and YS during summer occurred in the euphotic zone, and the highest  
206 concentrations occurred in waters at depths of 10–20 m (Fig. 5). The ratio of the mean Chl *a* concentration at depths  
207 of 10–20 m to depths > 60 m was 5.4. The depth distribution of DMS in seawater during summer decreased from the  
208 surface to the bottom seawater (Fig. 5). A significant depth gradient in the COS and CS<sub>2</sub> concentrations occurred at  
209 most stations, exhibiting decreases with the increasing depth. The ratios of the mean concentrations of COS, DMS,  
210 and CS<sub>2</sub> between the surface and depths > 60 m were 12.0, 8.6, and 11.5, respectively. However, the COS  
211 concentration was high in the bottom waters of station H16 (0.465 nmol L<sup>-1</sup>) (Fig. 5). The ratios of the mean  
212 concentrations of Chl *a*, COS, DMS, and CS<sub>2</sub> of all samples at different depths between summer and spring were 2.2,  
213 1.0, 5.6, and 2.0, respectively.

### 214 3.3 VSCs in the atmosphere

#### 215 3.3.1 Spring

216 The mixing ratios of COS, DMS, and CS<sub>2</sub> in the atmosphere overlying the BS and YS in spring were in the ranges of  
217 255.9–620.2 pptv, 1.3–191.2 pptv, and 5.2–698.8 pptv (Figs. 6a-6c), and their mean mixing ratios were  $345.6 \pm 79.2$   
218 pptv,  $47.5 \pm 49.8$  pptv, and  $113.2 \pm 172.3$  pptv, respectively. The decreasing order of the mean mixing ratios of the  
219 three VSCs in the atmosphere during spring was COS > CS<sub>2</sub> > DMS. The highest mixing ratio of atmospheric COS  
220 occurred at station B72 (Fig. 6a) near the northern Shandong Peninsula. The highest atmospheric DMS mixing ratio  
221 was observed at station B08 (Fig. 6b). The DMS concentration in the seawater (Fig. 2) was not as high as that in the  
222 atmosphere at station B49 (Fig. 6b). According to the 72 h backward trajectory map (Fig. S3), the air mass over station  
223 B49 had migrated from the land to the ocean, passing through Beijing, Tianjin, and other densely populated areas.  
224 The air mass over station B47 differed slightly from that over station B49 as it traversed the land of Liaoning province  
225 (12 h and 24 h backward trajectories in Fig. S3). The lowest atmospheric DMS mixing ratio was observed at station  
226 B47 (Fig. 6b), probably due to the low DMS concentration in seawater (0.5 nmol L<sup>-1</sup>) and the loss across the land. The  
227 highest atmospheric DMS mixing ratio occurred at station B08 (Fig. 6b). In addition, there were high mixing ratios of

228 CS<sub>2</sub> at stations in the BS, such as B57, B60, and B72, and low mixing ratios at stations B17 and B21 in the northern  
229 YS (Fig. 6c).

### 230 3.3.2 Summer

231 The mixing ratios of COS, DMS, and CS<sub>2</sub> in summer ranged from 394.6 to 850.1 pptv, from 10.3 to 464.3 pptv, and  
232 from 15.3 to 672.7 pptv, with mean values of  $563.8 \pm 168.9$  pptv,  $216.6 \pm 136.0$  pptv, and  $164.4 \pm 225.5$  pptv,  
233 respectively (Figs. 6d–6f). The order of the three VSCs in terms of the mean mixing ratios in the atmosphere during  
234 summer was COS > DMS > CS<sub>2</sub>. The ratios of the mean mixing ratios for atmospheric COS, DMS, and CS<sub>2</sub> between  
235 summer and spring were 1.6, 4.6, and 1.5, respectively. The three VSCs in the atmosphere over the BS and YS had  
236 similar spatial distributions. COS and DMS exhibited the highest mixing ratios at station B64 (Figs. 6d and 6e). The  
237 highest mixing ratio of CS<sub>2</sub> in summer appeared at station B49 near the shore, and the lowest one occurred far from  
238 shore at station H09 (Fig. 6f). The air masses over stations B49, B64, and H09 had migrated from the land, land, and  
239 ocean, respectively (Fig. S3). The distributions of CS<sub>2</sub> showed a decreasing trend from inshore to offshore (Fig. 6f).

### 240 3.4 Relationships between environmental factors and COS, DMS, and CS<sub>2</sub> concentrations

241 A significant correlation was found between the DMS and CS<sub>2</sub> concentrations in the surface seawater in spring ( $P <$   
242  $0.05$ ) and summer ( $P < 0.01$ ) (Table 1). A positive correlation occurred between the COS and DOC concentrations in  
243 seawater ( $P < 0.05$ ) and between the CS<sub>2</sub> and Chl *a* concentrations in seawater ( $P < 0.05$ ) during summer (Table 1).  
244 There was a significant correlation between the atmospheric COS and CS<sub>2</sub> mixing ratios in spring and summer ( $P <$   
245  $0.01$ , Table 1).

### 246 3.5 Sea-to-air fluxes of VSCs

#### 247 3.5.1 Spring

248 The sea-to-air fluxes of COS, DMS, and CS<sub>2</sub> in spring were 0.03–1.59, 0.06–25.40, and 0.003–0.30  $\mu\text{mol m}^{-2} \text{d}^{-1}$ , with  
249 averages of  $0.50 \pm 0.38$ ,  $2.99 \pm 4.24$ , and  $0.09 \pm 0.08$   $\mu\text{mol m}^{-2} \text{d}^{-1}$ , respectively (Fig. 7). The highest COS sea-to-air  
250 flux was observed at station B36, which had a high wind speed ( $11.3 \text{ m s}^{-1}$ ). In comparison, the lowest COS sea-to-air  
251 flux occurred at station B12, where the minimum wind speed occurred ( $1.5 \text{ m s}^{-1}$ ). The lowest sea-to-air fluxes of  
252 DMS and CS<sub>2</sub> occurred at stations H01 and B41 (Fig. 7), where the wind speeds were  $0.4 \text{ m s}^{-1}$  and  $2 \text{ m s}^{-1}$ , respectively.

253 The highest DMS and CS<sub>2</sub> sea-to-air fluxes appeared at stations HS4 and B68, respectively, due to high wind speeds  
254 and high DMS and CS<sub>2</sub> concentrations in seawater (Fig. 7).

### 255 **3.5.2 Summer**

256 The sea-to-air fluxes of COS, DMS, and CS<sub>2</sub> in summer were 0.06–1.51, 0.10–25.44, and 0.02–0.99  $\mu\text{mol m}^{-2} \text{d}^{-1}$ ,  
257 with averages of  $0.60 \pm 0.59$ ,  $6.26 \pm 6.27$ , and  $0.39 \pm 0.42 \mu\text{mol m}^{-2} \text{d}^{-1}$ , respectively, (Fig. 8). The ratios of the mean  
258 sea-to-air fluxes for COS, DMS, and CS<sub>2</sub> between summer and spring were 1.2, 2.1, and 4.3, respectively. Consistent  
259 with their order in seawater, the order of the sea-to-air fluxes of the VSCs was DMS > COS > CS<sub>2</sub>. The lowest sea-  
260 to-air fluxes of COS, DMS, and CS<sub>2</sub> in summer occurred at stations B64, B05, and B57, which had the low wind  
261 speeds of  $1 \text{ m s}^{-1}$ ,  $0.4 \text{ m s}^{-1}$ , and  $1.1 \text{ m s}^{-1}$ , respectively and low seawater VSC concentrations. The highest sea-to-air  
262 flux of COS and DMS occurred at stations B70 and H14, respectively, coinciding with high wind speeds and high  
263 COS and DMS concentrations in seawater (Fig. 8). The maximum CS<sub>2</sub> sea-to-air flux appeared at station H09, where  
264 the concentration of CS<sub>2</sub> in seawater was  $0.31 \text{ nmol L}^{-1}$  (Fig. 8).

## 265 **4 Discussion**

### 266 **4.1 Spatial and depth distributions and seasonal variations in VSCs in seawater**

#### 267 **4.1.1 Spatial distributions of VSCs and the impact factors**

268 The COS concentrations in this study were similar to those in six tidal European estuaries (Scheldt, Gironde, Rhine,  
269 Elbe, Ems, and Loire) ( $0.22 \text{ nmol L}^{-1}$ ) (Sciare et al., 2002), the DMS concentrations were lower than previous  
270 observations in the BS and YS in autumn ( $3.92 \text{ nmol L}^{-1}$ ) (Yang et al., 2014), and the CS<sub>2</sub> concentrations were lower  
271 than those in the coastal waters off the eastern coast of the United States ( $0.004\text{--}0.51 \text{ nmol L}^{-1}$ ) (Kim and Andreae,  
272 1992). Besides, the VSC concentrations in the seawater of the BS and YS were significantly higher than those in  
273 oceanic areas, such as the North Atlantic Ocean (Simó et al., 1997; Ulshöfer et al., 1995). The higher CDOM  
274 concentrations in the nearshore waters may be the reason for the difference (Gueguen et al., 2005). Zepp and Andreae  
275 (1994) demonstrated that photosensitized reaction of organosulfur compounds contributed to the production of COS.  
276 The reaction rates in coastal waters may be higher than those in open sea. Our results showed that the average COS,  
277 DMS, and CS<sub>2</sub> concentrations in the surface seawater of the BS and YS during summer were higher than those in the  
278 Changjiang estuary and the adjacent East China Sea (Yu et al., 2022). The reasons may be different sea areas,

279 temperatures, and industrial production. The mean concentrations of COS, DMS, and CS<sub>2</sub> in the surface seawater of  
280 the BS and YS during both spring and summer were 0.34, 3.41, 0.16 nmol L<sup>-1</sup>, respectively. The mean COS and CS<sub>2</sub>  
281 concentrations were approximately one order of magnitude higher than the global values reported by Lennartz et al.  
282 (2020), which were 32.3 pmol L<sup>-1</sup> and 15.7 pmol L<sup>-1</sup>. Lennartz et al. (2020) highlighted that the COS concentrations  
283 in estuaries and shelves were 10–1000 fold higher than those in oligotrophic waters. This disparity in concentrations  
284 may account for the discrepancies observed between our findings and global values. In comparison, the mean DMS  
285 concentration was similar with the value reported by Hulswar et al. (2022), which was 2.26 nmol L<sup>-1</sup>.

286 Different production and consumption mechanisms resulted in different spatial distributions of COS, DMS, and  
287 CS<sub>2</sub>. DMS and DMSP concentrations are related to the composition and abundance of phytoplankton (Kurian et al.,  
288 2020; Naik et al., 2020; O'Brien et al., 2022; Yu et al., 2023). The highest DMS concentrations at station B21 in spring  
289 coincided with high Chl *a* concentrations (Fig. 2). Low salinities (< 30) occurred at stations H25, H26, H34, H35,  
290 B43, B66, and B68 due to river water discharge from the Yangtze River Estuary, Yellow River, and Laizhou Bay in  
291 summer, consistent with the high nitrate, silicate, Chl *a*, and DMS concentrations (Figs. 3 and S2). High CS<sub>2</sub>  
292 concentrations in the coastal waters of the Yellow River estuary and at stations H18, H19, and B30 in spring may be  
293 due to high CDOM carried by the YS coastal current and Yellow River and terrestrial input. The significant correlation  
294 between the DMS and CS<sub>2</sub> concentrations in the surface seawater was consistent with the results of Ferek and Andreae  
295 (1983) and Yu et al. (2022). DMS in seawater is primarily derived from the degradation of DMSP, which is released  
296 from algal cell lysis (O'Brien et al., 2022). Moreover, the algae decay increased the CS<sub>2</sub> emission rate due to the  
297 degradation of sulfur-containing amino acids (Wang et al., 2023). The commonality of their sources resulted in a high  
298 correlation between the DMS and CS<sub>2</sub> concentrations in seawater. Xie et al. (1998) pointed out that CS<sub>2</sub> has a  
299 photochemical production mechanism similar to that of COS. Both are primarily produced by photochemical reactions  
300 of thiol-containing compounds, such as methyl mercaptan (MeSH) or glutathione, under the catalysis of CDOM.  
301 Terrestrial CDOM has higher photochemical reactivity and is more conducive to the photochemical generation of CS<sub>2</sub>  
302 (Xie et al., 1998). COS production rates increase with an increase in the absorption coefficient at 350 nm (*a*<sub>350</sub>) (Li et  
303 al., 2022). Uher and Andreae (1997) showed that the COS concentration in seawater was significantly correlated with  
304 the CDOM concentration. The positive correlation between the COS and DOC concentrations in seawater during  
305 summer in this study suggested that COS was produced by the photochemical reaction of CDOM. COS and CS<sub>2</sub> are  
306 formed via a reaction between cysteine and intermediates (i.e., CDOM, ·OH) (Chu et al., 2016; Du et al., 2017; Modiri

307 Gharehveran et al., 2020). Modiri Gharehveran and Shah (2021) showed that DOM could photochemically produce  
308  $^3\text{CDOM}^*$ ,  $^1\text{O}_2$ ,  $\text{H}_2\text{O}_2$ , and  $^{\bullet}\text{OH}$  by sunlight reacting with DMS, forming a sulfur- or carbon-centered radical and  
309 subsequently COS and  $\text{CS}_2$ . Li et al. (2022) demonstrated that a high nitrate concentration resulted in a high COS  
310 production rate. The high COS concentrations at stations H25 and B43 during summer coincided with high nitrate  
311 concentrations (Figs. 3 and S2). However, no significant correlations were found between the COS and nitrate  
312 concentrations during summer (Table 1).

#### 313 **4.1.2 Depth distributions of VSCs and impact factors**

314 The depth distributions of DMS, COS and  $\text{CS}_2$  showed similar patterns; their concentrations decreased with increasing  
315 depth, in agreement with the results of Yu et al. (2022). Yu et al. (2023) also showed that the DMS concentrations in  
316 the 35°N transect of the BS and YS in autumn decreased with an increase in seawater depth. The highest Chl *a*  
317 concentrations during summer occurred at depths of 10–20 m. This result was attributed to the abundance of nutrients  
318 and suitable water temperatures near the thermocline, benefitting phytoplankton growth. Yu et al. (2021) reported that  
319 the highest DMSP-consuming bacterial abundance and DMSP lyase activity at the 35°N transect in the summer of  
320 2013 occurred at depths of 10–15 m, consistent with our Chl *a* concentrations. DMS originates primarily from  
321 phytoplankton; thus, its concentration trend is similar to that of Chl *a*. COS and  $\text{CS}_2$  in seawater are predominantly  
322 derived from photochemical reactions of organic sulfides catalyzed by CDOM; therefore, light is the limiting factor  
323 for their production in seawater (Uher and Andreae, 1997). Ulshöfer et al. (1996) studied the depth distribution of  
324 COS in seawater and found that high COS concentrations occurred in the euphotic zone. The high COS concentrations  
325 in the surface seawater in this study may be attributed to the photochemical production reactions of  $\text{CS}_2$  and COS in  
326 the euphotic zone because they are dependent on light (Flöck et al., 1997; Xie et al., 1998). The addition of  
327 photosensitizers-natural DOM and commercial humic acid (HA) photo-catalyzed glutathione (GSH) and cysteine, and  
328 enhanced the COS formation (Flöck et al., 1997). An excited triplet state CDOM ( $^3\text{CDOM}^*$ ) is produced by COS in  
329 the presence of ultraviolet light (Li et al., 2022). In addition, the loss processes include exhalation, downward mixing,  
330 and hydrolysis, with hydrolysis being identified as the predominant sink (Xu et al., 2001). We speculate that slow  
331 hydrolysis rate may be another reason accounting for the high COS concentrations in the surface seawater. Hobe et  
332 al. (2001) stated that the non-photochemical production of COS is critical for the global budget. Consistent with Hobe  
333 et al. (2001), the high COS concentration in the bottom waters at station H16 in summer may be related to the non-  
334 photochemical production of COS or release by underlying sediments. Consistent with our  $\text{CS}_2$  results, Xie et al. (1998)

335 showed that the CS<sub>2</sub> concentrations decreased with the depth, coinciding with solar radiation changes. Decreased  
336 photochemical reaction due to decreasing solar radiation with water depth may explain the vertical distribution of CS<sub>2</sub>  
337 (Xie et al., 1998). Similar to the results of Xie et al. (1998), the high CS<sub>2</sub> concentrations in the bottom seawater at  
338 station H15 in spring may be attributable to a sedimentary source.

#### 339 **4.1.3 Seasonal and diurnal variations in VSCs in seawater**

340 The VSCs in seawater exhibited significant seasonal differences (VSCs in summer > VSCs in spring) in this study.  
341 Similar seasonal variations in COS were also observed by Xu et al. (2001), who found that the COS concentrations in  
342 South Africa were higher in summer than in autumn. In addition, observations by Weiss et al. (1995) showed that the  
343 COS concentrations in the seawater of the Atlantic and Pacific Oceans were very low in winter. Xu et al. (2001)  
344 concluded that warmer seasons and high biological productivity resulted in enhanced COS concentrations. The  
345 significant correlation between the oceanic COS concentrations and the temperatures in spring (Table 1) can prove  
346 this. Xie et al. (1998) showed that the order of the CS<sub>2</sub> production rates was summer > spring > fall > winter. The  
347 significant positive correlations between the CS<sub>2</sub> and Chl *a* concentrations during summer may explain the higher CS<sub>2</sub>  
348 concentration in seawater during summer than during spring in this study. Similar to the seasonal changes in Chl *a*,  
349 the DMS concentrations were higher in summer than in spring. A higher phytoplankton biomass in summer has been  
350 linked to higher DMS concentrations in summer than in autumn (Yang et al., 2015). In addition, diurnal variations in  
351 the COS concentrations in seawater (high during the daytime and low at night) were reported (Ferek and Andreae,  
352 1984; Lennartz et al., 2017; Xu et al., 2001). COS photoproduction via photochemical reactions is more rapid than  
353 hydrolysis during the daytime (Xu et al., 2001). Furthermore, the COS concentration depends on the light intensity  
354 (Ferek and Andreae, 1984). Therefore, the sampling time can influence the measured COS concentrations in the  
355 seawater.

#### 356 **4.2 VSCs in the atmosphere**

357 The mean mixing ratios of COS and CS<sub>2</sub> in the atmosphere overlying the BS and YS during both spring and summer  
358 were 411.0 and 128.6 pptv, respectively. These values were 0.75-fold and 3.05-fold of the global scale values reported  
359 by Lennartz et al. (2020), which were 548.9 ppt and 42.2 ppt. Similar to our results for the VSC mixing ratios in the  
360 atmosphere during summer, Kettle et al. (2001) found that the COS mixing ratio in the Atlantic Ocean atmosphere  
361 was 552 pptv, while Cooper and Saltzman (1993) measured a DMS mixing ratio of 118 pptv. In addition, the mixing

362 ratios of atmospheric CS<sub>2</sub> in this study were similar to those in a polluted atmosphere (Sandalls and Penkett, 1977)  
363 but much higher than those in unpolluted atmospheres, such as over the North Atlantic (Cooper and Saltzman, 1993).  
364 This finding indicated that industrial production and human activities significantly affect the mixing ratios of CS<sub>2</sub> in  
365 the atmosphere. The mean VSC mixing ratios in the atmosphere during summer in this study were all higher than  
366 those in the Changjiang estuary and the adjacent East China Sea (Yu et al., 2022), and the Western Pacific during  
367 autumn (Xu et al., 2023).

368 No significant correlation was found between the oceanic VSC concentrations and atmospheric VSC mixing ratios  
369 (Table 1). The reason may be that VSCs in the atmosphere were not only derived from sea-to-air diffusion but also  
370 from anthropogenic sources, such as the soil, incomplete burning of biomass, and industrial releases (Blake et al.,  
371 2004; Chin and Davis, 1993; Whelan et al., 2018). Anthropogenic VSC emissions can be evaluated using isotope  
372 measurements (Hattori et al., 2020). However, anthropogenic VSCs emissions were not evaluated in this study, and  
373 isotope measurements will be obtained in future studies. The highest mixing ratios of atmospheric COS at station B72  
374 and DMS at station B08 in spring coincided with anthropogenic emissions and high DMS concentration in seawater,  
375 respectively (Fig. 6). The CS<sub>2</sub> generated by industrial activities may have influenced the atmosphere at station B49,  
376 which is near industrial cities, such as Tianjin. Chemical production and pharmaceutical industries are large emitters  
377 of CS<sub>2</sub> into the atmosphere (Chin and Davis, 1993). CS<sub>2</sub> is the main precursor of COS in the atmosphere, and  
378 atmospheric CS<sub>2</sub> is oxidized to COS by radicals such as OH with a conversion efficiency of 0.81 (Chin and Davis,  
379 1995). The significant correlation between atmospheric COS and CS<sub>2</sub> in our study (Table 1) demonstrated this.

380 The tropospheric lifetime of COS, CS<sub>2</sub>, and DMS were found to be 2–7 years, several days, and approximately 24  
381 h, respectively (Lennartz et al., 2020; Khan et al., 2016). Backward trajectories in 12, 24, and 72 h were used to  
382 identify the sources of these compounds in our study (Fig. S3). The 72 h backward trajectories showed that air masses  
383 from different sources (land or ocean) and passing through different regions may have affected the atmospheric COS,  
384 DMS, and CS<sub>2</sub> mixing ratios. Jiang et al. (2021) stated that different sources of air masses might have affected  
385 atmospheric DMS oxidation to MSA. The 72 h backward trajectory over station B49 indicated that the high  
386 atmospheric DMS mixing ratio was attributable to human activities. The wind direction is from continental Asia to  
387 the Pacific in spring. The backward trajectories of B49, B47, and B08 showed that anthropogenic and oceanic DMS  
388 emissions accounted for the atmospheric DMS sources. The wind direction of the air mass from the back trajectories



389 of Miyakojima, Yokohama, and Otaru in Japan in winter (January to March) observed by Hattori et al. (2020) was  
390 similar to ours in spring (March to April). Hattori et al. (2020) reported that the anthropogenic COS originated  
391 primarily from the Chinese industry and was transported by air to southern Japan. The backward trajectory of H09  
392 showed that the wind direction was from the south of Taiwan Island in summer, and oceanic sources accounted for  
393 the atmospheric DMS. The air masses showed that the highest mixing ratios of COS and DMS at station B64 in  
394 summer were caused by terrestrial sources from northeast China and oceanic sources in the BS, respectively. The  
395 highest CS<sub>2</sub> mixing ratio in summer at station B49 may be due to the air mass transported from the northeast, i.e.,  
396 industrial cities in China.

### 397 **4.3 Sea-to-air fluxes of VSCs**

398 The mean sea-to-air fluxes of DMS in spring ( $2.99 \mu\text{mol S m}^{-2} \text{d}^{-1}$ ) and summer ( $6.26 \mu\text{mol S m}^{-2} \text{d}^{-1}$ ) observed in our  
399 study fell within the range of global DMS fluxes, which ranged from 0 to  $10 \mu\text{mol S m}^{-2} \text{d}^{-1}$  (Hulswar et al., 2022).  
400 The calculated DMS sea-to-air fluxes in our study should be seen as upper limits due to setting the atmospheric mixing  
401 ratio to be zero. The spatial variability in the sea-to-air fluxes was consistent with changes in the wind speed because  
402 sea-to-air fluxes depend on the transmission velocities of VSCs in seawater, which are related to the wind speed and  
403 viscosity of seawater. In addition, the sea-to-air fluxes of all three VSCs were positive in spring and summer, indicating  
404 that the seawater was a source of COS, DMS, and CS<sub>2</sub> to the atmosphere through sea-to-air diffusion. Although our  
405 findings agree with those of Chin and Davis (1993) and Yu et al. (2022), who showed that the ocean was a major  
406 atmospheric source of COS, they conflict with the results of Weiss et al. (1995) and Zhu et al. (2019), who found  
407 significant COS undersaturation in some sea areas. Therefore, the ocean may be a sink of atmospheric COS in some  
408 areas or at certain times of the year.

## 409 **5 Conclusions**

410 The COS, DMS, and CS<sub>2</sub> distributions in the surface seawater and marine atmosphere of the BS and YS during spring  
411 and summer exhibited significant spatial and seasonal variability. First, the COS, DMS, and CS<sub>2</sub> concentrations were  
412 higher in summer than in spring. Second, the COS, DMS, and CS<sub>2</sub> concentrations were the highest in the surface  
413 seawater and decreased with the depth. The positive correlation between the oceanic COS and DOC concentrations in  
414 summer suggested the photochemical production of COS from CDOM. In addition, the atmospheric VSC mixing  
415 ratios of the BS and YS exhibited substantial seasonal differences, with higher mixing ratios in summer than in spring.

416 There was a significant correlation between the atmospheric COS and CS<sub>2</sub> mixing ratios, which may verify the COS  
417 production from oxidation of CS<sub>2</sub>. The backward trajectories showed that the atmospheric mixing ratios of VSCs were  
418 affected by anthropogenic and/or oceanic emissions. Finally, the high sea-to-air fluxes of COS, DMS, and CS<sub>2</sub> in the  
419 BS and YS indicated that marginal seas are important sources of atmospheric VSCs and may contribute considerably  
420 to the global sulfur budget.

421 *Data availability.* Data to support this article are available at <https://doi.org/10.6084/m9.figshare.14971644>.

422 *Author contributions.* All authors were involved in the writing of the paper and approved the final submitted paper.

423 YJ and YL were major contributors to the study's conception, data analysis and drafting of the paper. HZ, LJG and  
424 LQ contributed significantly to writing-original draft. YGP contributed to writing-reviewing, and editing.

425 *Competing interests.* The authors declare that they have no conflict of interest.

426 *Acknowledgements.* We are grateful to the captain and crew of the R/V “Dong Fang Hong 2” for their help and  
427 cooperation during the in situ investigation.

428 *Financial support.* This work was funded by the National Natural Science Foundation of China (41976038, 41876122),  
429 and the National Key Research and Development Program (2016YFA0601301).

## 430 **References**

431 Andreae, M. O., and Crutzen, P. J.: Atmospheric aerosols: biogeochemical sources and role in atmospheric chemistry,  
432 *Science*, 276 (5315), 1052–1058, <https://doi.org/10.1126/science.276.5315.1052>, 1997.

433 Aydin, M., Britten, G. L., Montzka, S. A., Buizert, C., Primeau, F. W., Petrenko, V. V., Battle, M. O., Nicewonger,  
434 M. R., Patterson, J., Hmiel, B., and Saltzman, E. S.: Anthropogenic impacts on atmospheric carbonyl sulfide since  
435 the 19th century inferred from polar firn air and ice core measurements, *J. Geophys. Res.-Atmos.*, 125(16),  
436 e2020JD033074, <https://doi.org/10.1002/essoar.10503126.1>, 2020.

437 Blake, N. J., Streets, D. G., Woo, J.-H., Simpson, I. J., Green, J., Meinardi, S., Kita, K., Atlas, E., Fuelberg, H. E.,  
438 Sachse, G., Avery, M. A., Vay, S. A., Talbot, R. W., Dibb, J. E., Bandy, A. R., Thornton, D. C., Rowland, F. S.,  
439 and Blake, D. R.: Carbonyl sulfide and carbon disulfide: large-scale distributions over the western Pacific and  
440 emissions from Asia during TRACE-P, *J. Geophys. Res.-Atmos.*, 109, D15S05,  
441 <https://doi.org/10.1029/2003JD004259>, 2004.

442 Brown, A. S., van der Veen, A. M. H., Arrhenius, K., Murugan, A., Culleton, L. P., Ziel, P. R., and Li, J.: Sampling

443 of gaseous sulfur-containing compounds at low concentrations with a review of best-practice methods for biogas  
444 and natural gas applications, *Trac-Trends Anal. Chem.*, 64, 42–52, <https://doi.org/10.1016/j.trac.2014.08.012>, 2015.

445 Brühl, C., Lelieveld, J., Crutzen, P. J., and Tost, H.: The role of carbonyl sulphide as a source of stratospheric sulphate  
446 aerosol and its impact on climate, *Atmos. Chem. Phys.*, 12(3), 1239–1253, [http://dx.doi.org/10.5194/acp-12-1239-](http://dx.doi.org/10.5194/acp-12-1239-2012)  
447 2012, 2012.

448 Campbell, J. E., Carmichael, G. R., Chai T., Mena-Carrasco, M., Tang, Y., Blake, D. R., Blake, N. J., Vay, S. A.,  
449 Collatz, G. J., Baker, I., Berry, J. A., Montzka, S. A., Sweeney, C., Schnoor, J. L., and Stanier, C. O.: Photosynthetic  
450 control of atmospheric carbonyl sulfide during the growing season, *Science*, 322, 1085–1088,  
451 <https://doi.org/10.1126/science.1164015>, 2008.

452 Campbell, J. E., Whelan, M. E., Seibt U., Smith S. J., Berry, J. A., and Hilton, T. W.: Atmospheric carbonyl sulfide  
453 sources from anthropogenic activity: Implications for carbon cycle constraints, *Geophys. Res. Lett.*, 42, 3004–3010,  
454 <https://doi.org/10.1002/2015GL063445>, 2015.

455 Charlson, R. J., Lovelock, J. E., Andreae, M. O., and Warren, S. G.: Oceanic phytoplankton, atmospheric sulphur,  
456 cloud albedo and climate, *Nature*, 326, 655–661, <https://doi.org/10.1038/326655a0>, 1987.

457 Chen C.-T. A.: Chemical and physical fronts in the Bohai, Yellow and East China seas, *J. Mar. Syst.*, 78(3), 394–410,  
458 <https://doi.org/10.1016/j.jmarsys.2008.11.016>, 2009.

459 Chen, Y., Wang, P., Shi, D., Ji, C.-X., Chen, R., Gao, X.-C., and Yang, G.-P.: Distribution and bioavailability of  
460 dissolved and particulate organic matter in different water masses of the Southern Yellow Sea and East China Sea,  
461 *J. Marine Syst.*, 222, 103596, <https://doi.org/10.1016/j.jmarsys.2021.103596>, 2021.

462 Chin, M., and Davis, D. D.: Global sources and sinks of OCS and CS<sub>2</sub> and their distributions, *Global Biogeochem.*  
463 *Cy.*, 7(2), 321–337, <https://doi.org/10.1029/93GB00568>, 1993.

464 Chin, M., and Davis, D. D.: A reanalysis of carbonyl sulfide as a source of stratospheric background sulfur aerosol, *J.*  
465 *Geophys. Res.-Atmos.*, 100(D5), 8993–9005, <https://doi.org/10.1029/95JD00275>, 1995.

466 Chu, C., Erickson, P. R., Lundeen, R. A., Stamatelatos, D., Alaimo, P. J., Latch D. E., and McNeill, K.: Photochemical  
467 and nonphotochemical transformations of cysteine with dissolved organic matter, *Environ. Sci. Technol.*, 50, 6363–  
468 6373, <https://doi.org/10.1021/acs.est.6b01291>, 2016.

469 Cline, J. D., and Bates, T. S.: Dimethyl sulfide in the Equatorial Pacific Ocean: a natural source of sulfur to the  
470 atmosphere, *Geophys. Res. Lett.*, 10(10), 949–952, <https://doi.org/10.1029/GL010i010p00949>, 1983.

471 Cooper, D. J., and Saltzman, E. S.: Measurements of atmospheric dimethylsulfide, hydrogen sulfide, and carbon  
472 disulfide during GTE/CITE 3, *J. Geophys. Res.-Atmos.*, 98(D12), 23397–23409,  
473 <https://doi.org/10.1029/92JD00218>, 1993.

474 Crutzen, P. J.: The possible importance of CSO for the sulfate layer of the stratosphere, *Geophys. Res. Lett.*, 3(2), 73–  
475 76, <https://doi.org/10.1029/GL003i002p00073>, 1976.

476 Curson, A. R. J., Liu, J., Bermejo Martínez, A., Green, R. T., Chan, Y., Carrión, O., Williams, B. T., Zhang, S.-H.,  
477 Yang, G.-P., Bulman Page, P. C., Zhang, X.-H., and Todd, J. D.: Dimethylsulfoniopropionate biosynthesis in marine  
478 bacteria and identification of the key gene in this process, *Nat. Microbiol.*, 2: 17009,  
479 <https://doi.org/10.1038/nmicrobiol.2017.9>, 2017.

480 Dacey, J. W. H., Wakeham, S. G., and Howes, B. L.: Henry's law constants for dimethylsulfide in freshwater and  
481 seawater, *Geophys. Res. Lett.*, 11, 991–994, <https://doi.org/10.1029/GL011i010p00991>, 1984.

482 De Bruyn, W. J., Swartz, E., Hu, J. H., Shorter, J. A., Davidovits, P., Worsnop, D. R., Zahniser, M. S., and Kolb, C.  
483 E.: Henry's law solubilities and Setchenow coefficients for biogenic reduced sulfur species obtained from gas-liquid  
484 uptake measurements, *J. Geophys. Res.-Atmos.*, 100, 7245–7251, <https://doi.org/10.1029/95JD00217>, 1995.

485 Du, Q., Mu, Y., Zhang, C., Liu, J., Zhang, Y., and Liu, C.: Photochemical production of carbonyl sulfide, carbon  
486 disulfide and dimethyl sulfide in a lake water, *J. Environ. Sci.*, 51, 146–156,  
487 <https://doi.org/10.1016/j.jes.2016.08.006>, 2017.

488 Ferek, R. J., and Andreae, M. O.: Photochemical production of carbonyl sulphide in marine surface waters. *Nature*,  
489 307, 148–150, <https://doi.org/10.1038/307148a0>, 1984.

490 Ferek, R. J., and Andreae, M. O.: The supersaturation of carbonyl sulfide in surface waters of the Pacific Ocean off  
491 Peru, *Geophys. Res. Lett.*, 10(5), 393–396, <https://doi.org/10.1029/GL010I005P00393>, 1983.

492 Flöck, O. R., Andreae, M. O., and Dräger, M.: Environmentally relevant precursors of carbonyl sulfide in aquatic  
493 systems, *Mar. Chem.*, 59(1-2), 71–85, [https://doi.org/10.1016/S0304-4203\(97\)00012-1](https://doi.org/10.1016/S0304-4203(97)00012-1), 1997.

494 Guéguen, C., Guo, L., and Tanaka, N.: Distributions and characteristics of colored dissolved organic matter in the

495 Western Arctic Ocean, *Cont. Shelf Res.*, 25, 1195–1207, <https://doi.org/10.1016/j.csr.2005.01.005>, 2005.

496 Hattori, S., Kamezaki, K., and Yoshida, N.: Constraining the atmospheric OCS budget from sulfur isotopes, *Proc.*  
497 *Natl. Acad. Sci. U.S.A.*, 117(34), 20447–20452, <https://doi.org/10.1073/pnas.2007260117>, 2020.

498 Hobe, M. V., Cutter, G. A., Kettle, A. J., and Andreae, M. O.: Dark production: a significant source of oceanic COS,  
499 *J. Geophys. Res.-Oceans.*, 106(C12), 31217–31226, <https://doi.org/10.1029/2000JC000567>, 2001.

500 Hulswar, S., Sim ó R., Gal í M., Bell, T. G., Lana, A., Inamdar, S., Halloran, P. R., Manville, G., and Mahajan, A. S.:  
501 Third revision of the global surface seawater dimethyl sulfide climatology (DMS-Rev3), *Earth Syst. Sci. Data*, 14,  
502 2963–2987, <https://doi.org/10.5194/essd-14-2963-2022>, 2022.

503 Inomata, Y., Hayashi, M., Osada, K., and Iwasaka, Y.: Spatial distributions of volatile sulfur compounds in surface  
504 seawater and overlying atmosphere in the northwestern Pacific Ocean, eastern Indian Ocean, and Southern Ocean,  
505 *Global Biogeochem. Cy.*, 20(2), GB2022, <https://doi.org/10.1029/2005GB002518>, 2006.

506 Jiang, B., Xie, Z., Qiu, Y., Wang, L., Yue, F., Kang, H., Yu, X., and Wu, X.: Modification of the conversion of  
507 dimethylsulfide to methanesulfonic acid by anthropogenic pollution as revealed by long-term observations, *ACS*  
508 *Earth Space Chem.*, 5, 2839–2845, <https://doi.org/10.1021/acsearthspacechem.1c00222>, 2021.

509 Keller, M. D., Bellows, W. K., and Guillard, R. R. L.: Dimethyl sulfide production in marine phytoplankton, in:  
510 *Biogenic sulfur in the environment*, edited by: Millero, F. J., Hershey, J. P., Saltzman, E. S., and Cooper, W. J.,  
511 American Chemical Society, Washington, DC, 167–182, <http://dx.doi.org/10.1021/bk-1989-0393.ch011>, 1989.

512 Kettle, A. J., Kuhn, U., von Hobe, M., Kesselmeier, J., and Andreae, M. O.: Global budget of atmospheric carbonyl  
513 sulfide: temporal and spatial variations of the dominant sources and sinks, *J. Geophys. Res.*, 107(D22), 4658,  
514 <https://doi.org/10.1029/2002JD002187>, 2002.

515 Kettle, A. J., Rhee, T. S., von Hobe, M., Poulton, A., Aiken, J., and Andreae, M. O.: Assessing the flux of different  
516 volatile sulfur gases from the ocean to the atmosphere, *J. Geophys. Res.-Atmos.*, 106(D11), 12193–12209,  
517 <https://doi.org/10.1029/2000JD900630>, 2001.

518 Khan, M. A. H., Gillespie, S. M. P., Razis, B., Xiao, P., Davies-Coleman, M. T., Percival, C. J., Derwent, R. G., Dyke,  
519 J. M., Ghosh, M. V., Lee, E. P. F., and Shallcross, D. E.: A modelling study of the atmospheric chemistry of DMS  
520 using the global model, STOCHEM-CRI, *Atmos. Environ.*, 127, 69–79.

521 <http://dx.doi.org/10.1016/j.atmosenv.2015.12.028>, 2016.

522 Kim, K.-H., and Andreae, M. O.: Carbon disulfide in estuarine, coastal and oceanic environments, *Mar. Chem.*, 40,  
523 179–197, [https://doi.org/10.1016/0304-4203\(92\)90022-3](https://doi.org/10.1016/0304-4203(92)90022-3), 1992.

524 Kurian S, Chndrasekhararao A. V., Vidya P. J., Shenoy D. M., Gauns M., Uskaikar, H., and Aparna, S. G.: Role of  
525 oceanic fronts in enhancing phytoplankton biomass in the eastern Arabian Sea during an oligotrophic period, *Mar.*  
526 *Environ. Res.*, 160, 105023, <https://doi.org/10.1016/j.marenvres.2020.105023>, 2020.

527 Lennartz, S. T., Gauss, M., von Hobe, M., and Marandino, C. A.: Monthly resolved modelled oceanic emissions of  
528 carbonyl sulphide and carbon disulphide for the period 2000–2019, *Earth Syst. Sci. Data*, 13, 2095–2110,  
529 <https://doi.org/10.5194/essd-13-2095-2021>, 2021.

530 Lennartz, S. T., Marandino, C. A., von Hobe, M., Andreae, M. O., Aranami, K., Atlas, E., Berkelhammer, M.,  
531 Bingemer, H., Booge, D., Cutter, G., Cortes, P., Kremser, S., Law, C. S., Marriner, A., Simó R., Quack, B., Uher,  
532 G., Xie, H., and Xu, X.: Marine carbonyl sulfide (OCS) and carbon disulfide (CS<sub>2</sub>): a compilation of measurements  
533 in seawater and the marine boundary layer, *Earth Syst. Sci. Data*, 12, 591–609, [https://doi.org/10.5194/essd-12-](https://doi.org/10.5194/essd-12-591-2020)  
534 [591-2020](https://doi.org/10.5194/essd-12-591-2020), 2020.

535 Lennartz, S. T., Marandino, C. A., von Hobe, M., Cortes, P., Quack, B., Simo, R., Booge, D., Pozzer, A., Steinhoff,  
536 T., Arevalo-Martinez, D. L., Kloss, C., Bracher, A., Röttgers, R., Atlas, E., and Krüger, K.: Direct oceanic emissions  
537 unlikely to account for the missing source of atmospheric carbonyl sulfide, *Atmos. Chem. Phys.*, 17, 385–402,  
538 <https://doi.org/10.5194/acp-17-385-2017>, 2017.

539 Li, J.-L., Zhai, X., and Du, L.: Effect of nitrate on the photochemical production of carbonyl sulfide from surface  
540 seawater, *Geophys. Res. Lett.*, 49, e2021GL097051, <https://doi.org/10.1029/2021GL097051>, 2022.

541 Liss, P. S., and Slater, P. G.: Flux of gases across the air-sea interface, *Nature*, 247(5438), 181–184,  
542 <https://doi.org/10.1038/247181a0>, 1974.

543 Logan, J. A., McElroy, M. B., Wofsy, S. C., and Prather, M. J.: Oxidation of CS<sub>2</sub> and COS: sources for atmospheric  
544 SO<sub>2</sub>. *Nature* 281, 185–188. <https://doi.org/10.1038/281185a0>, 1979.

545 Maignan, F., Abadie, C., Remaud, M., Kooijmans, L. M. J., Kohonen, K.-M., Commane, R., Wehr, R., Campbell, J.  
546 E., Belviso, S., Montzka, S. A., Raoult, N., Seibt, U., Shiga, Y. P., Vuichard, N., Whelan, M. E., and Peylin, P.:  
547 Carbonyl sulfide: comparing a mechanistic representation of the vegetation uptake in a land surface model and the

548 leaf relative uptake approach, *Biogeosciences*, 18, 2917–2955, <https://doi.org/10.5194/bg-18-2917-2021>, 2021.

549 Modiri Gharehveran, M., Hain E, Blaney L, and Shah, A. D.: Influence of dissolved organic matter on carbonyl sulfide  
550 and carbon disulfide formation from cysteine during sunlight photolysis, *Environ. Sci.: Processes Impacts*, 22,  
551 1852–1864, <https://doi.org/10.1039/D0EM00219D>, 2020.

552 Modiri Gharehveran, M., and Shah, A. D.: Influence of dissolved organic matter on carbonyl sulfide and carbon  
553 disulfide formation from dimethyl sulfide during sunlight photolysis, *Water Environ. Res.*, 93, 2982–2997,  
554 <https://doi.org/10.1002/wer.1650>, 2021.

555 Naik, B. R., Gauns, M., Bepari, K., Uskaikar, H., and Shenoy, D. M.: Variation in phytoplankton community and its  
556 implication to dimethylsulphide production at a coastal station off Goa, India, *Mar. Environ. Res.*, 157, 104926,  
557 <https://doi.org/10.1016/j.marenvres.2020.104926>, 2020.

558 Nightingale, P. D., Malin, G., Law, C. S., Watson, A. J., Liss, P. S., Liddicoat, M. I., Boutin, J., and Upstill-Goddard,  
559 R. C.: In situ evaluation of air-sea gas exchange parameterizations using novel conservative and volatile tracers,  
560 *Global Biogeochem. Cy.*, 14(1), 373–387, <https://doi.org/10.1029/1999GB900091>, 2000.

561 O'Brien, J., McParland, E. L., Bramucci, A. R., Ostrowski, M., Siboni, N., Ingleton, T., Brown, M. V., Levine, N. M.,  
562 Laverock, B., Petrou, K., and Seymour, J.: The microbiological drivers of temporally dynamic  
563 dimethylsulfoniopropionate cycling processes in Australian coastal shelf waters, *Front. Microbiol.*, 13, 894026,  
564 <https://doi.org/10.3389/fmicb.2022.894026>, 2022.

565 Parsons, T. R., Maita, Y., and Lalli, C. M.: A manual of chemical and biological methods for seawater analysis, in  
566 Fluorometric determination of chlorophylls, edited by: Parsons, T. R., Maita, Y., and Lalli, C. M., Great Britain,  
567 CA: Pergamon Press, 107–109, 1984.

568 Reisch, C. R., Stoudemayer, M. J., Varaljay, V. A., Amster, I. J., Moran, M. A., and Whitman, W. B.: Novel pathway  
569 for assimilation of dimethylsulphoniopropionate widespread in marine bacteria, *Nature*, 473(7346), 208–211,  
570 <https://doi.org/10.1038/nature10078>, 2011.

571 Remaud, M., Chevallier, F., Maignan, F., Belviso, S., Berchet, A., Parouffe, A., Abadie, C., Bacour, C., Lennartz, S.,  
572 and Peylin, P.: Plant gross primary production, plant respiration and carbonyl sulfide emissions over the globe  
573 inferred by atmospheric inverse modelling, *Atmos. Chem. Phys.*, 22(4), 2525–2552, [https://doi.org/10.5194/acp-](https://doi.org/10.5194/acp-22-2525-2022)  
574 [22-2525-2022](https://doi.org/10.5194/acp-22-2525-2022), 2022.

575 Sandalls, F. J., and Penkett, S. A.: Measurements of carbonyl sulphide and carbon disulphide in the atmosphere, *Atmos.*  
576 *Environ.*, 11(2), 197–199, [https://doi.org/10.1016/0004-6981\(77\)90227-X](https://doi.org/10.1016/0004-6981(77)90227-X), 1977.

577 Sander, R.: Compilation of Henry's law constants (version 4.0) for water as solvent, *Atmos. Chem. Phys.*, 15, 4399–  
578 4981, <https://doi.org/10.5194/acp-15-4399-2015>, 2015.

579 Schäfer, H., Myronova, N., and Boden, R.: Microbial degradation of dimethylsulphide and related C<sub>1</sub>-sulphur  
580 compounds: organisms and pathways controlling fluxes of sulphur in the biosphere, *J. Exp. Bot.*, 61(2), 315–334,  
581 <https://doi.org/10.1093/jxb/erp355>, 2010.

582 Schlitzer, R.: Ocean Data View, [odv.awi.de](http://odv.awi.de), 2023.

583 Sciare, J., Mihalopoulos, N., and Nguyen, B. C.: Spatial and temporal variability of dissolved sulfur compounds in  
584 European estuaries, *Biogeochemistry*, 59(1–2), 121–141, <http://dx.doi.org/10.1023/A:1015539725017>, 2002.

585 Simó, R., Grimalt, J. O., and Albaigés, J.: Dissolved dimethylsulphide, dimethylsulphoniopropionate and  
586 dimethylsulphoxide in western Mediterranean waters, *Deep-Sea Res. Pt II*, 44(3-4), 929–950,  
587 [https://doi.org/10.1016/S0967-0645\(96\)00099-9](https://doi.org/10.1016/S0967-0645(96)00099-9), 1997.

588 Staubes, R., and Georgii, H.-W.: Biogenic sulfur compounds in seawater and the atmosphere of the Antarctic region,  
589 *Tellus B*, 45(2), 127–137, <https://doi.org/10.3402/tellusb.v45i2.15587>, 1993.

590 Tian, X., Hu, M., and Ma, Q.: Determination of volatile sulfur compounds in the atmosphere and surface seawater in  
591 Qingdao, *Acta Scien. Circum.*, 25(1), 30–33, (in Chinese with English abstract),  
592 <https://doi.org/10.13671/j.hjkxxb.2005.01.005>, 2005.

593 Turner, S. M., Malin, G., Nightingale, P. D., and Liss, P. S.: Seasonal variation of dimethyl sulphide in the North Sea  
594 and an assessment of fluxes to the atmosphere, *Mar. Chem.*, 54(3–4), 245–262, [https://doi.org/10.1016/0304-](https://doi.org/10.1016/0304-4203(96)00028-X)  
595 [4203\(96\)00028-X](https://doi.org/10.1016/0304-4203(96)00028-X), 1996.

596 Uher, G., and Andreae, M. O.: Photochemical production of carbonyl sulfide in North Sea water: a process study,  
597 *Limnol. Oceanogr.*, 42(3), 432–442, <https://doi.org/10.4319/lo.1997.42.3.0432>, 1997.

598 Ulshöfer, V. S., Flöck, O. R., Uher, G., and Andreae, M. O.: Photochemical production and air-sea exchange of  
599 carbonyl sulfide in the eastern Mediterranean Sea, *Mar. Chem.*, 53(53), 25–39, [https://doi.org/10.1016/0304-](https://doi.org/10.1016/0304-4203(96)00010-2)  
600 [4203\(96\)00010-2](https://doi.org/10.1016/0304-4203(96)00010-2), 1996.



601 Ulshöfer, V. S., Uher, G., and Andreae, M. O.: Evidence for a winter sink of atmospheric carbonyl sulfide in the  
602 northeast Atlantic Ocean, *Geophys. Res. Lett.*, 22(19), 2601–2604, <https://doi.org/10.1029/95GL02656>, 1995.

603 Wang, J., Chu, Y.-X., Tian, G., and He, R.: Estimation of sulfur fate and contribution to VSC emissions from lakes  
604 during algae decay, *Sci. Total Environ.*, 856, 159193, <http://dx.doi.org/10.1016/j.scitotenv.2022.159193>, 2023.

605 Watts, S. F.: The mass budgets of carbonyl sulfide, dimethyl sulfide, carbon disulfide and hydrogen sulfide, *Atmos.*  
606 *Environ.*, 34, pp. 761–779, [https://doi.org/10.1016/S1352-2310\(99\)00342-8](https://doi.org/10.1016/S1352-2310(99)00342-8), 2000.

607 Weiss, P. S., Johnson, J. E., Gammon, R. H., and Bates, T. S.: Reevaluation of the open ocean source of carbonyl  
608 sulfide to the atmosphere, *J. Geophys. Res.-Atmos.*, 100(D11), 23083–23092, <https://doi.org/10.1029/95JD01926>,  
609 1995.

610 Whelan, M. E., Lennartz, S. T., Gimeno, T. E., Wehr, R., Wohlfahrt, G., Wang, Y., Kooijmans, L. M. J., Hilton, T.  
611 W., Belviso, S., Peylin, P., Commane, R., Sun, W., Chen, H., Kuai, L., Mammarella, I., Maseyk, K., Berkelhammer,  
612 M., Li, K.-F., Yakir, D., Zumkehr, A., Katayama, Y., Ogée, J., Spielmann, F. M., Kitz, F., Rastogi, B., Kesselmeier,  
613 J., Marshall, J., Erkkilä K.-M., Wingate, L., Meredith, L. K., He, W., Bunk, R., Launois, T., Vesala, T., Schmidt,  
614 J. A., Fichot, C. G., Seibt, U., Saleska, S., Saltzman, E. S., Montzka, S. A., Berry, J. A., and Campbell, J. E.:  
615 Reviews and syntheses: carbonyl sulfide as a multi-scale tracer for carbon and water cycles, *Biogeosciences*, 15,  
616 3625–3657, <https://doi.org/10.5194/bg-15-3625-2018>, 2018.

617 Xie, H., Moore, R. M., and Miller, W. L.: Photochemical production of carbon disulphide in seawater, *J. Geophys.*  
618 *Res.-Oceans*, 103(C3), 5635–5644, <https://doi.org/10.1029/97JC02885>, 1998.

619 Xu, F., Zhang, H.-H., Yan, S.-B., Sun, M.-X., Wu, J.-W., and Yang, G.-P.: Biogeochemical controls on climatically  
620 active gases and atmospheric sulfate aerosols in the western Pacific, *Environ. Res.*, 220, 115211,  
621 <https://doi.org/10.1016/j.envres.2023.115211>, 2023.

622 Xu, X., Bingemer, H. G., Georgii, H.-W., Schmidt, U., and Bartell, U.: Measurements of carbonyl sulfide (COS) in  
623 surface seawater and marine air, and estimates of the air-sea flux from observations during two Atlantic cruises, *J.*  
624 *Geophys. Res.-Atmos.*, 106(D4), 3491–3502, <https://doi.org/10.1029/2000JD900571>, 2001.

625 Yang, G.-P., Jing, W.-W., Kang, Z.-Q., Zhang, H.-H., and Song, G.-S.: Spatial variations of dimethylsulfide and  
626 dimethylsulfoniopropionate in the surface microlayer and in the subsurface waters of the South China Sea during  
627 springtime, *Mar. Environ. Res.*, 65, 85–97, <https://doi.org/10.1016/j.marenvres.2007.09.002>, 2008.

628 Yang, G.-P., Song, Y.-Z., Zhang, H.-H., Li, C.-X., and Wu, G.-W.: Seasonal variation and biogeochemical cycling of  
629 dimethylsulfide (DMS) and dimethylsulfoniopropionate (DMSP) in the Yellow Sea and Bohai Sea, *J. Geophys.*  
630 *Res.-Oceans*, 119(12), 8897–8915, <https://doi.org/10.1002/2014JC010373>, 2014.

631 Yang, G.-P., Zhang, S.-H., Zhang, H.-H., Yang, J., and Liu, C.-Y.: Distribution of biogenic sulfur in the Bohai Sea  
632 and northern Yellow Sea and its contribution to atmospheric sulfate aerosol in the late fall, *Mar. Chem.*, 169, 23–  
633 32, <https://doi.org/10.1016/j.marchem.2014.12.008>, 2015.

634 Yu, J., Zhang, S.-H., Tian, J.-Y., Zhang, Z.-Y., Zhao, L.-J., Xu, R., Yang, G.-P., Lai, J.-G., Wang, X.-D.: Distribution  
635 and dimethylsulfoniopropionate degradation of dimethylsulfoniopropionate-consuming bacteria in the Yellow Sea  
636 and East China Sea, *J. Geophys. Res.-Oceans*, 126, e2021JC017679, <https://doi.org/10.1029/2021JC017679>, 2021.

637 Yu, J., Sun, M.-X., and Yang, G.-P.: Occurrence and emissions of volatile sulfur compounds in the Changjiang estuary  
638 and the adjacent East China Sea, *Mar. Chem.*, 238, 104062, <https://doi.org/10.1016/j.marchem.2021.104062>, 2022.

639 Yu, J., Wang, S., Lai, J.-G., Tian, J.-Y., Zhang, H.-Q., Yang, G.-P., and Chen, R.: The effect of zooplankton on the  
640 distributions of dimethyl sulfide and dimethylsulfoniopropionate in the Bohai and Yellow Seas, *J. Geophys. Res.-*  
641 *Oceans*, 128, e2022JC019030, <https://doi.org/10.1029/2022JC019030>, 2023.

642 Zepp, R. G., and Andreae, M. O.: Factors affecting the photochemical production of carbonyl sulfide in seawater,  
643 *Geophys. Res. Lett.*, 21(25), 2813–2816, <https://doi.org/10.1029/94GL03083>, 1994.

644 Zhang, Y., Tan, D.-D., He, Z., Yu, J., Yang, G.-P.: Dimethylated sulfur, methane and aerobic methane production in  
645 the Yellow Sea and Bohai Sea, *J. Geophys. Res.-Oceans*, 128, e2023JC019736,  
646 <https://doi.org/10.1029/2023JC019736>, 2023.

647 Zhang, S.-H., Yang, G.-P., Zhang, H.-H., and Yang, J.: Spatial variation of biogenic sulfur in the south Yellow Sea  
648 and the East China Sea during summer and its contribution to atmospheric sulfate aerosol, *Sci. Total Environ.*, 488-  
649 489, 157–167, <https://doi.org/10.1016/j.scitotenv.2014.04.074>, 2014.

650 Zhao, Y., Schlundt, C., Booge, D., and Bange, H. W.: A decade of dimethyl sulfide (DMS),  
651 dimethylsulfoniopropionate (DMSP) and dimethyl sulfoxide (DMSO) measurements in the southwestern Baltic Sea,  
652 *Biogeosciences*, 18, 2161–2179, <https://doi.org/10.5194/bg-18-2161-2021>, 2021.

653 Zhu, R., Yang, G.-P., and Zhang, H.-H.: Temporal and spatial distributions of carbonyl sulfide, dimethyl sulfide, and

654 carbon disulfide in seawater and marine atmosphere of the Changjiang Estuary and its adjacent East China Sea,  
655 *Limnol. Oceanogr.*, 64, 632–649, <https://doi.org/10.1002/lno.11065>, 2019.

656 Zhu, R., Zhang, H.-H., and Yang, G.-P.: Determination of volatile sulfur compounds in seawater and atmosphere,  
657 *Chin. J. Anal. Chem.*, 45(10), 1504–1510, (in Chinese with English abstract), [https://doi.org/10.11895/j.issn.0253-](https://doi.org/10.11895/j.issn.0253-3820.170291)  
658 3820.170291, 2017.

659 Zumkehr, A., Hilton, T. W., Whelan, M., Smith, S., Kuai, L., Worden, J., and Campbell, J. E.: Global gridded  
660 anthropogenic emissions inventory of carbonyl sulfide, *Atmos. Environ.*, 183, 11–19,  
661 <https://doi.org/10.1016/j.atmosenv.2018.03.063>, 2018.

662

663 **Figure captions**

664 **Fig. 1.** Sampling stations in the Yellow Sea and Bohai Sea during (a) spring and (b) summer (▲ indicates stations  
665 where atmospheric samples were collected). Yellow Sea Cold Water Mass: YSCWM. The maps were plotted with  
666 Ocean Data View (ODV software) (Schlitzer, 2023).

667 **Fig. 2.** Spatial distributions of temperature, salinity, Chl *a*, COS, DMS, CS<sub>2</sub>, and DOC in the surface water of the BS  
668 and YS in spring.

669 **Fig. 3.** Spatial distributions of temperature, salinity, Chl *a*, COS, DMS, CS<sub>2</sub>, and DOC in the surface water of the BS  
670 and YS in summer.

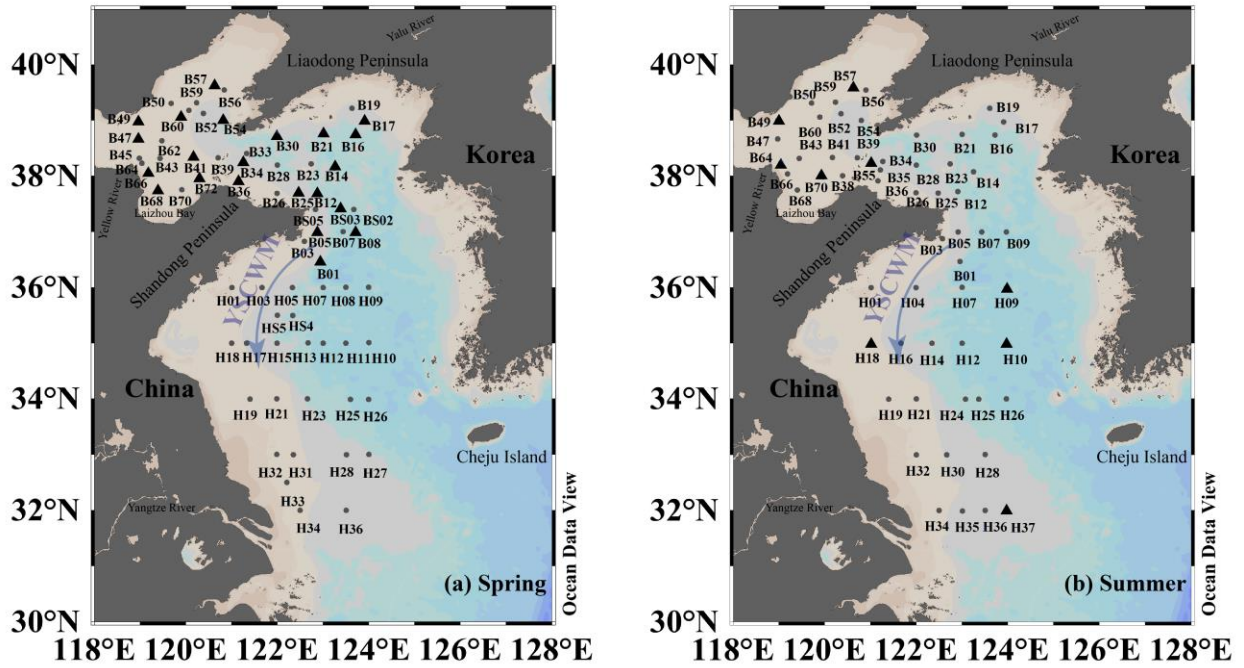
671 **Fig. 4.** Depth distributions of temperature, salinity, Chl *a*, COS, DMS, and CS<sub>2</sub> in seawater in spring.

672 **Fig. 5.** Depth distributions of temperature, salinity, Chl *a*, COS, DMS, and CS<sub>2</sub> in seawater in summer.

673 **Fig. 6.** Spatial distributions of COS, DMS, and CS<sub>2</sub> in the atmosphere over the BS and YS in (a)–(c) spring and (d)–(f)  
674 summer. (Unit: pptv)

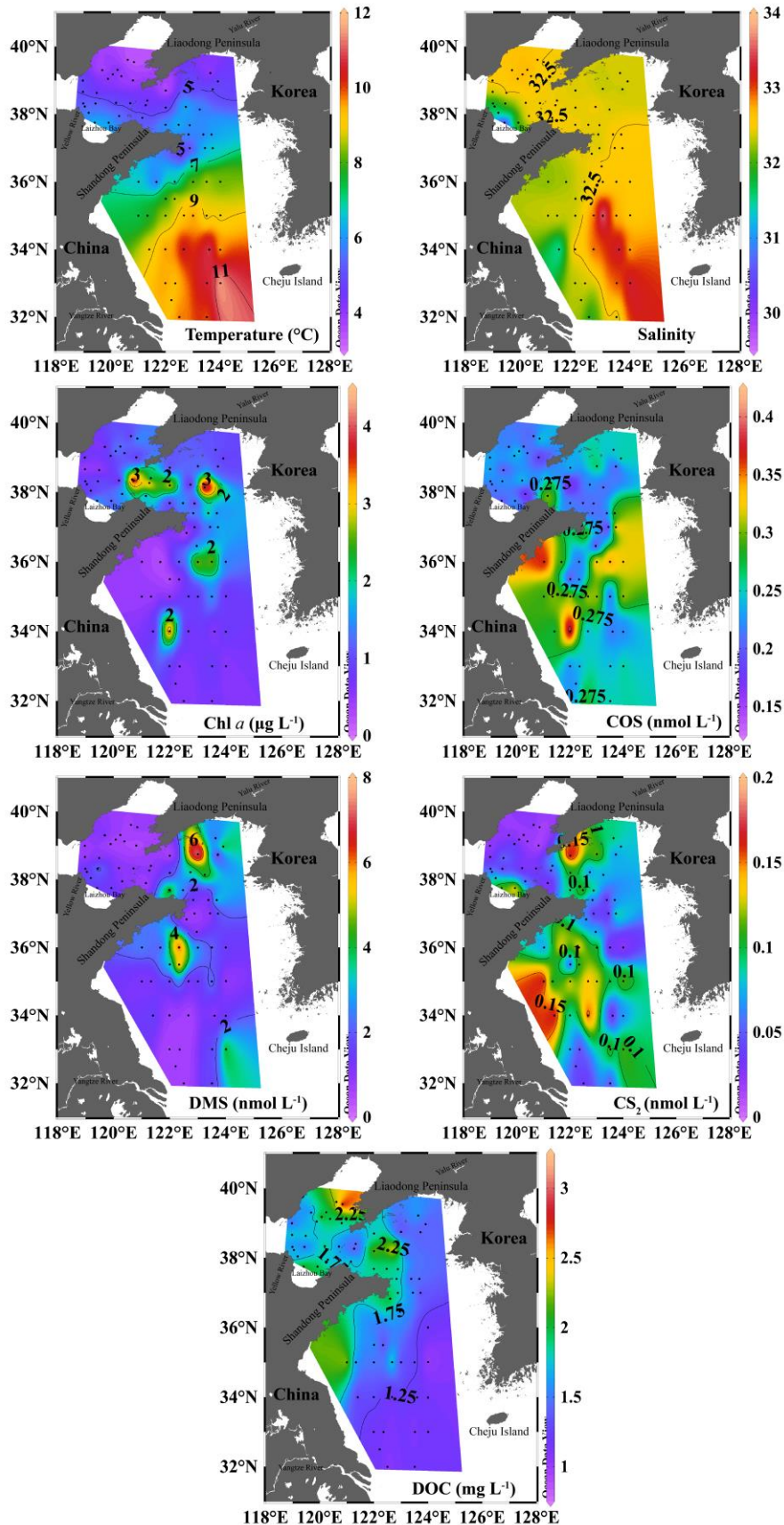
675 **Fig. 7.** Variations in sea-to-air fluxes of VSCs, VSCs concentrations in seawater, and wind speeds in the BS and YS  
676 in spring 2018.

677 **Fig. 8.** Variations in sea-to-air fluxes of VSCs, VSCs concentrations in seawater, and wind speeds in the BS and YS  
678 in summer 2018.  
679

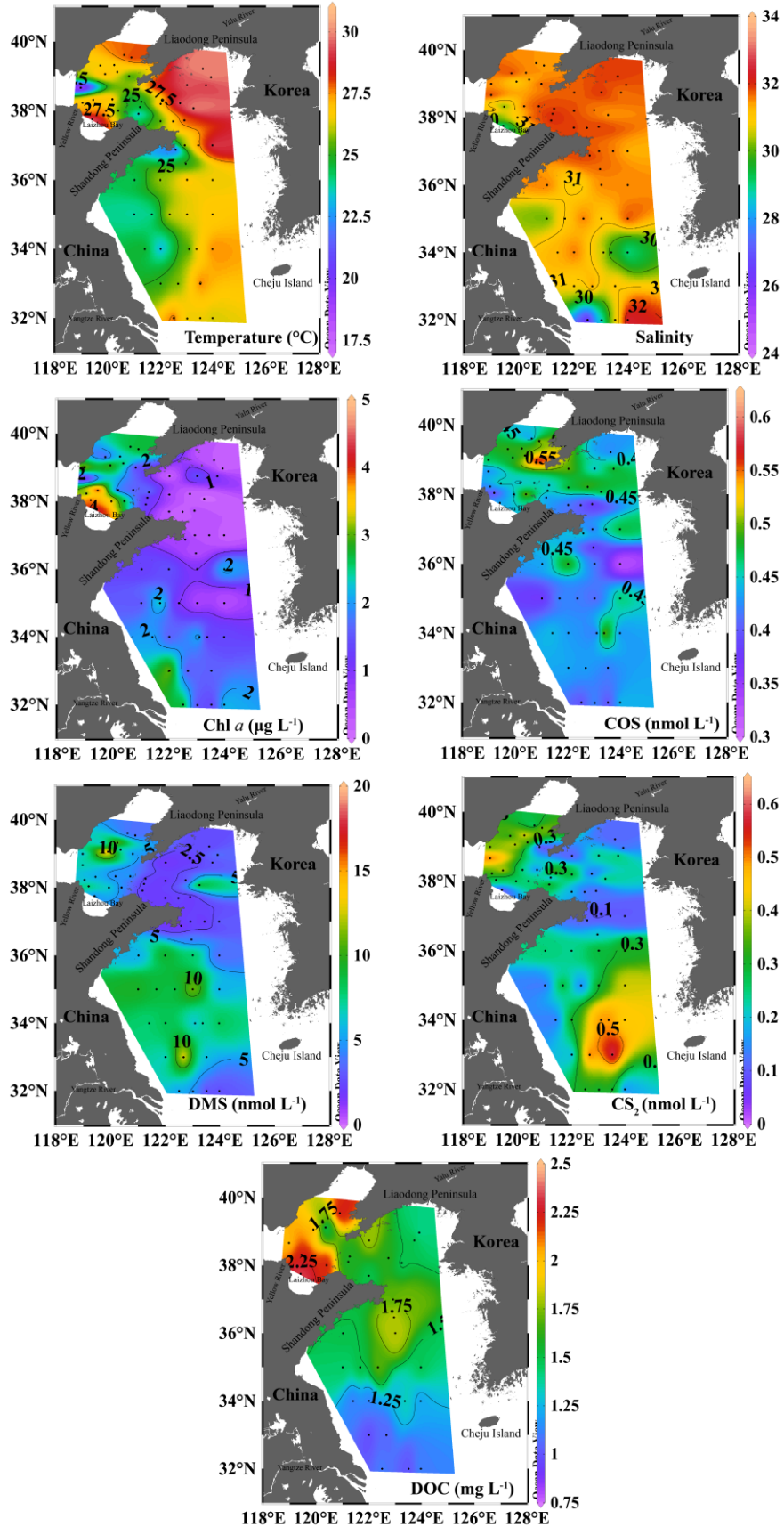


681  
682  
683  
684  
685

**Fig. 1.** Sampling stations in the Yellow Sea and Bohai Sea during (a) spring and (b) summer (▲ indicates stations where atmospheric samples were collected). Yellow Sea Cold Water Mass: YSCWM. The maps were plotted with Ocean Data View (ODV software) (Schlitzer, 2023).



687 **Fig. 2.** Spatial distributions of temperature, salinity, Chl *a*, COS, DMS, CS<sub>2</sub>, and DOC in the surface water of the BS  
688 and YS in spring.





690 **Fig. 3.** Spatial distributions of temperature, salinity, Chl *a*, COS, DMS, CS<sub>2</sub>, and DOC in the surface water of the BS  
691 and YS in summer.

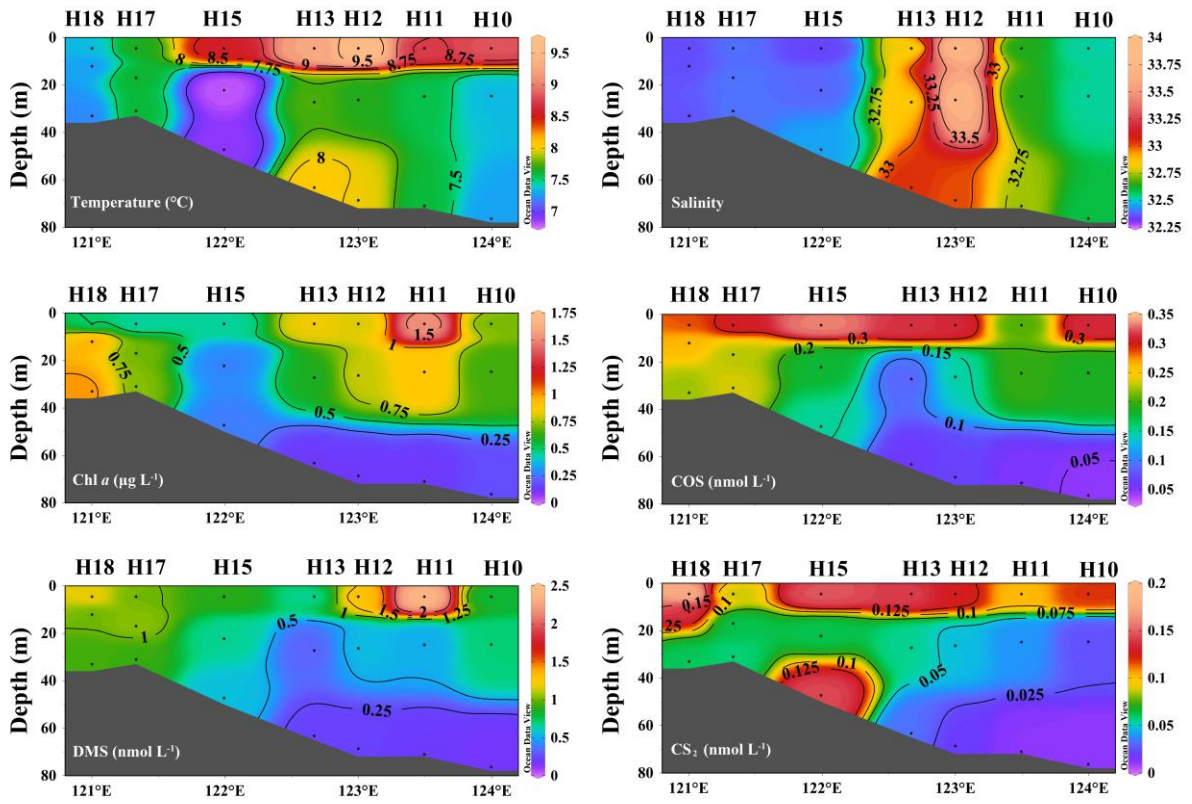
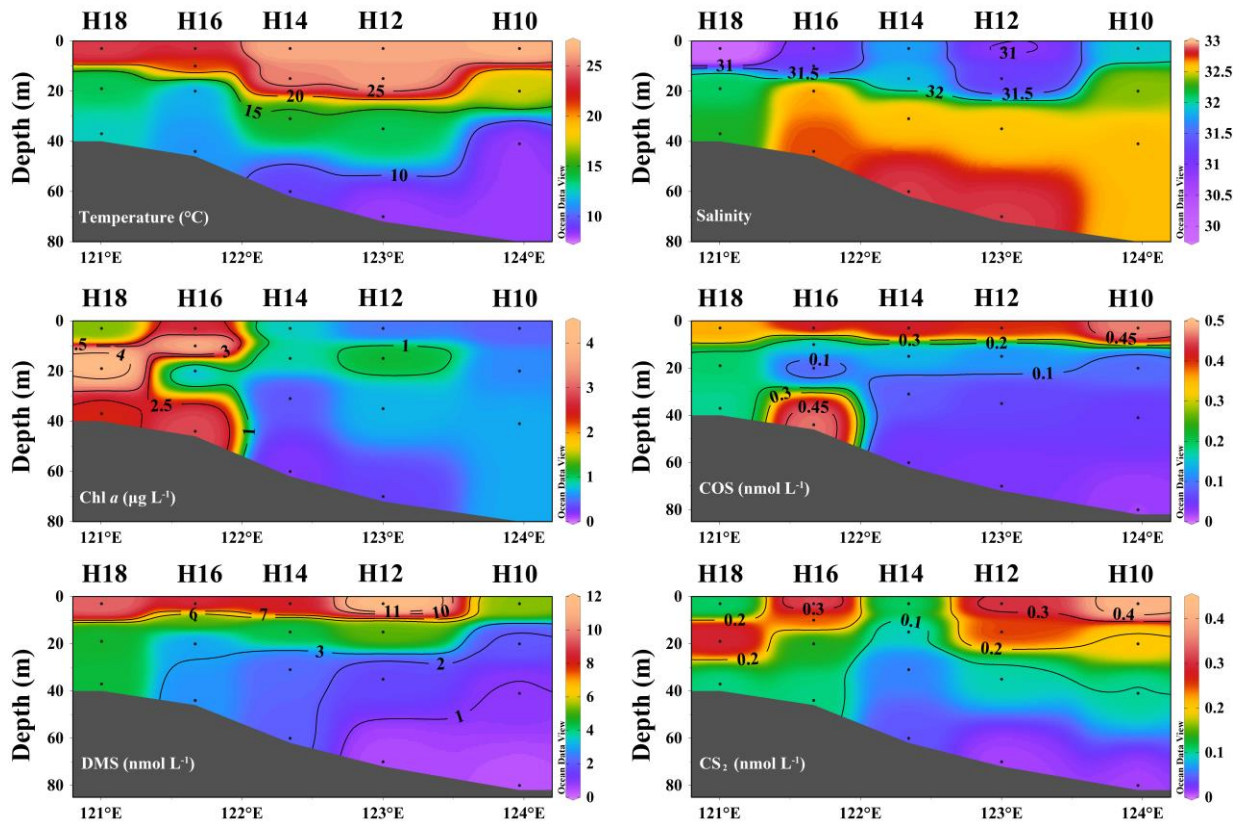


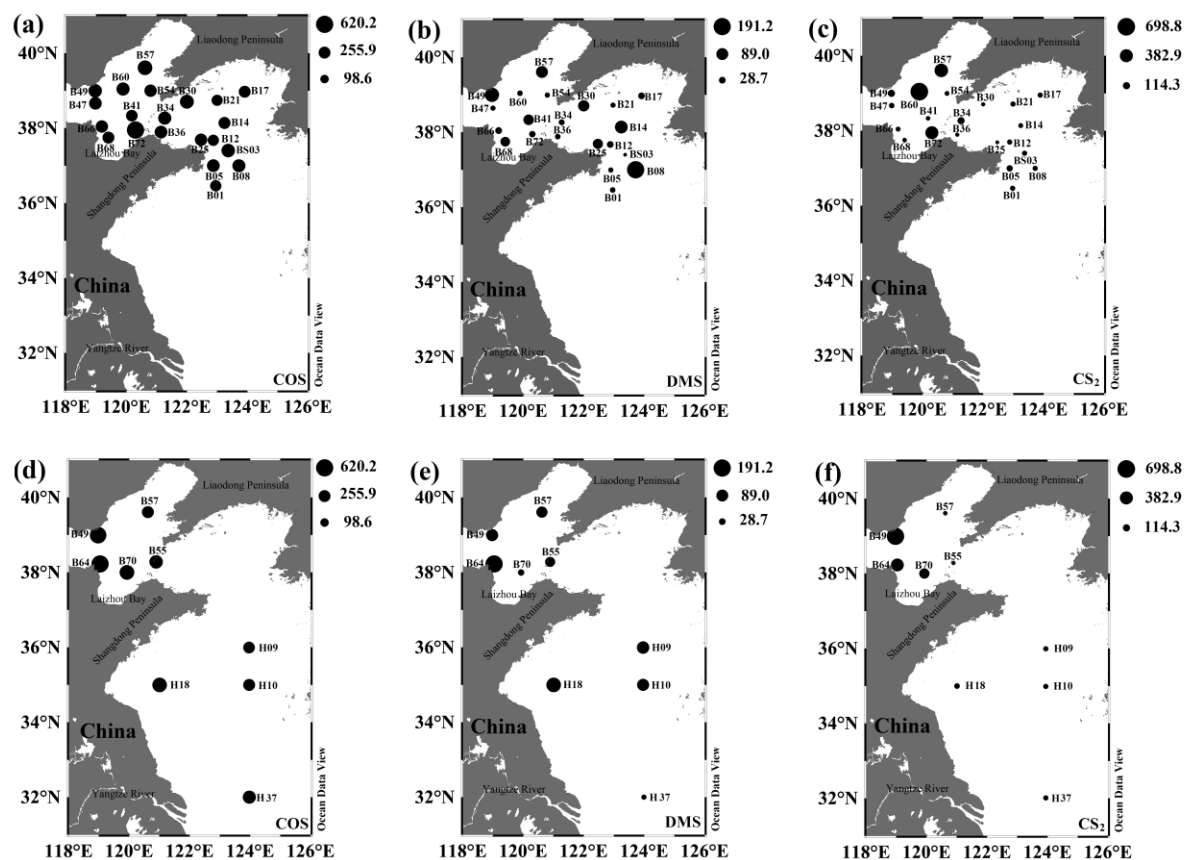
**Fig. 4.** Depth distributions of temperature, salinity, Chl *a*, COS, DMS, and CS<sub>2</sub> in seawater in spring.

692  
693  
694

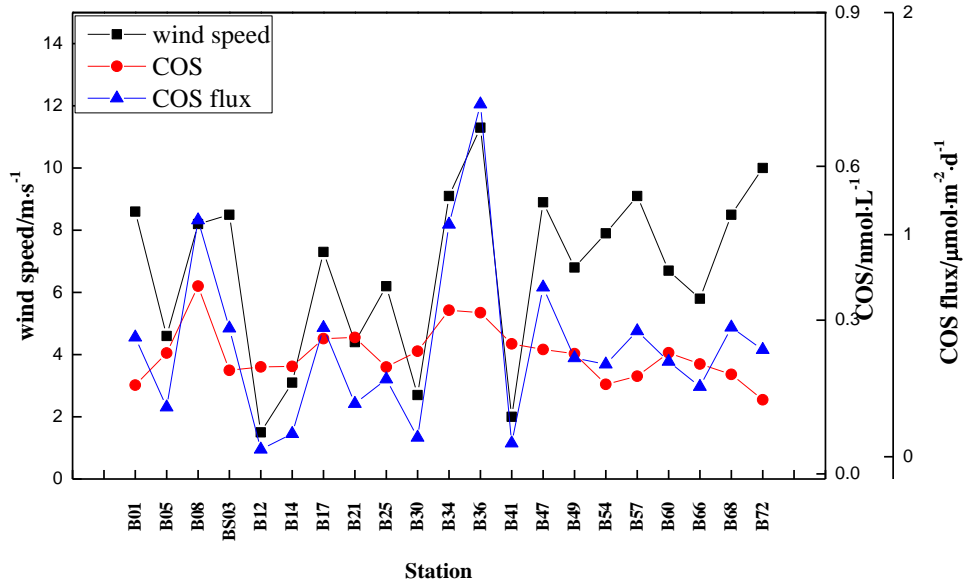


695  
696  
697

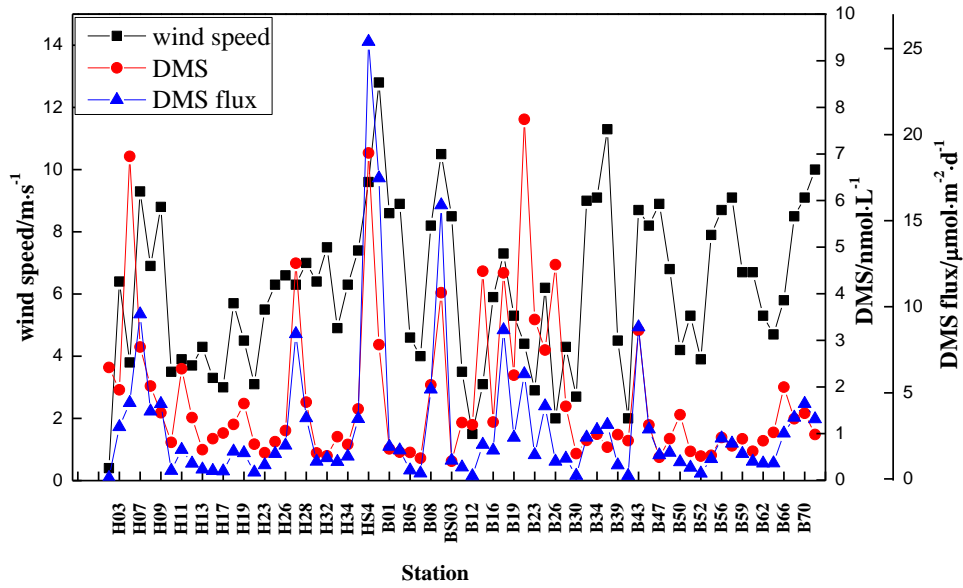
**Fig. 5.** Depth distributions of temperature, salinity, Chl *a*, COS, DMS, and CS<sub>2</sub> in seawater in summer.



698  
 699 **Fig. 6.** Spatial distributions of COS, DMS, and CS<sub>2</sub> in the atmosphere over the BS and YS in (a)–(c) spring and (d)–(f)  
 700 summer. (Unit: pptv)

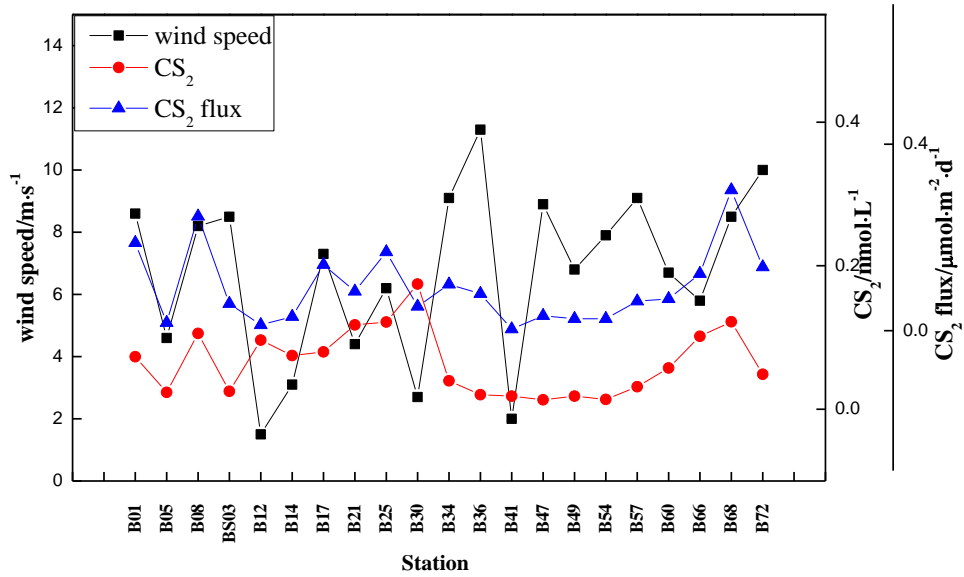


701



702

703

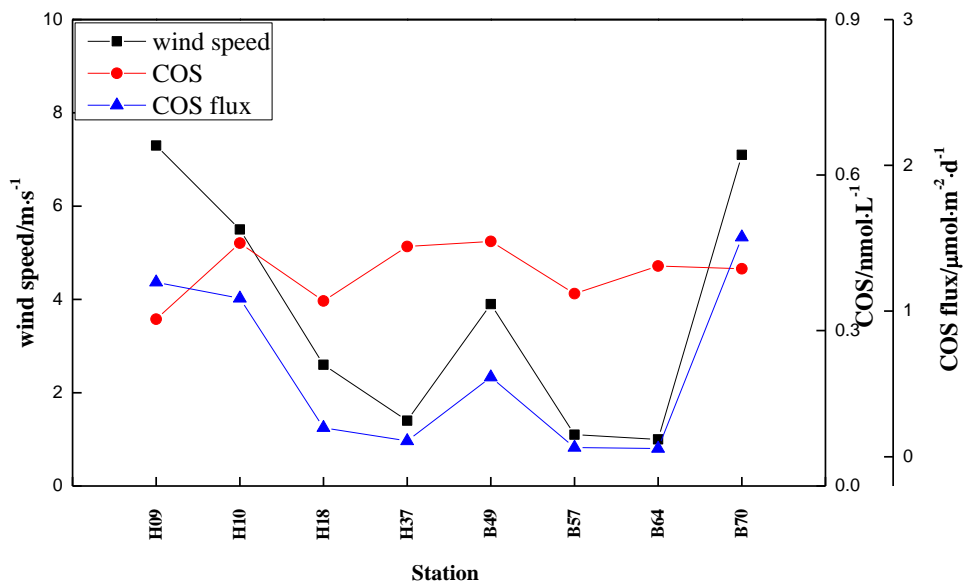


704

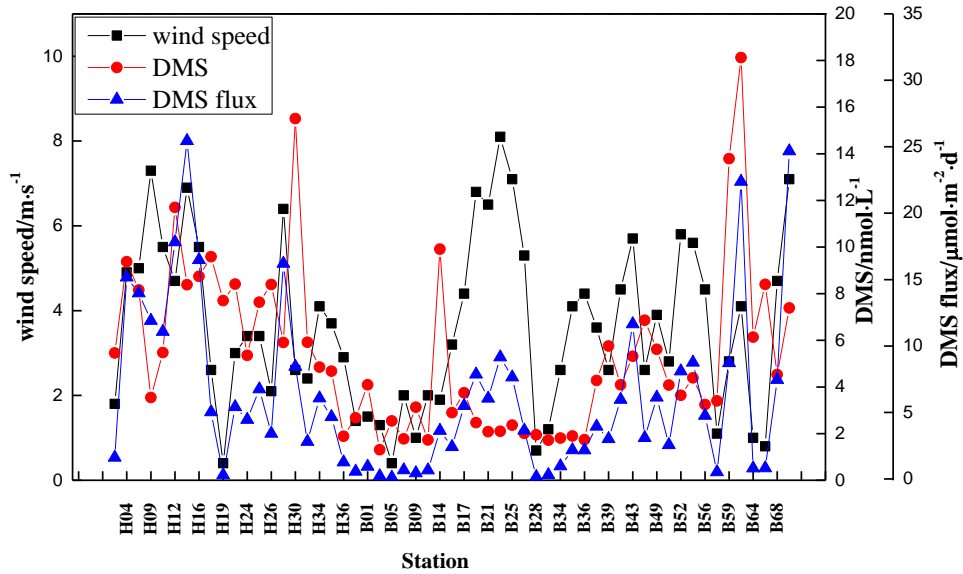
705 **Fig. 7.** Variations in sea-to-air fluxes of VSCs, VSCs concentrations in seawater, and wind speeds in the BS and YS

706

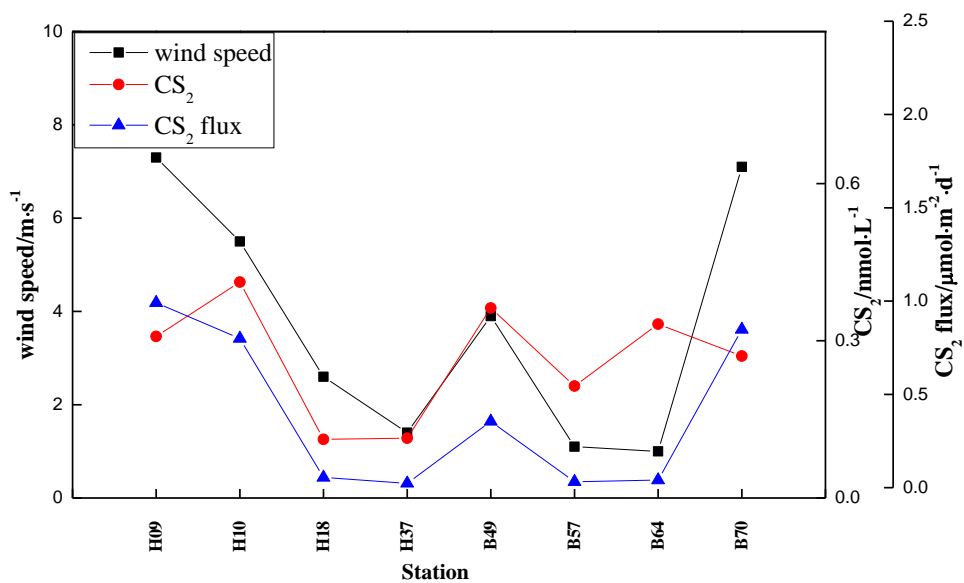
in spring 2018.



707  
708



709



710  
 711 **Fig. 8.** Variations in sea-to-air fluxes of VSCs, VSCs concentrations in seawater, and wind speeds in the BS and YS  
 712 in summer 2018.



713 **Table 1** Correlation analyses of the three VSCs and environmental factors in the BS and YS in spring and summer.

Spring	COS (seawater)	DMS (seawater)	CS <sub>2</sub> (seawater)	COS (atmosphere)	DMS (atmosphere)	CS <sub>2</sub> (atmosphere)
COS (seawater)	1					
DMS (seawater)	0.021	1				
CS <sub>2</sub> (seawater)	0.193	0.281*	1			
COS (atmosphere)	-0.246	-0.355	-0.182	1		
DMS (atmosphere)	0.296	0.04	0.274	0.117	1	
CS <sub>2</sub> (atmosphere)	-0.201	-0.264	-0.213	0.554**	-0.013	1
Chl <i>a</i>	0.132	0.044	-0.095	0.033	0.179	-0.141
Temperature	0.286*	0.082	0.319**	-0.257	0.179	-0.372
Salinity	0.11	-0.009	-0.109	0.24	0.019	0.236
Silicate	-0.103	-0.252*	-0.029	0.351	-0.008	0.54
Phosphate	-0.084	-0.205	-0.353**	0.621	-0.128	0.36
Nitrate	-0.299*	-0.293*	-0.226	0.075	-0.096	0.044
DOC	-0.146	-0.153	-0.073	0.037	-0.122	0.008
Summer	COS (seawater)	DMS (seawater)	CS <sub>2</sub> (seawater)	COS (atmosphere)	DMS (atmosphere)	CS <sub>2</sub> (atmosphere)
COS (seawater)	1					
DMS (seawater)	0.009	1				
CS <sub>2</sub> (seawater)	-0.007	0.424**	1			
COS (atmosphere)	0.358	0.472	0.184	1		
DMS (atmosphere)	-0.266	0.404	0.31	0.451	1	
CS <sub>2</sub> (atmosphere)	0.452	0.229	0.424	0.855**	0.251	1
Chl <i>a</i>	-0.059	0.25	0.274*	0.461	-0.294	0.565
Temperature	0.088	-0.076	-0.143	-0.097	-0.349	0.072
Salinity	0.128	-0.172	-0.143	-0.12	-0.352	-0.044
Silicate	0.114	0.122	0.276*	0.312	-0.548	0.377
Phosphate	0.104	-0.169	-0.245	-0.49	-0.539	-0.482
Nitrate	-0.095	0.145	0.057	-0.008	0.224	-0.155
DOC	0.342*	-0.015	0.012	0.02	0.924	0.319

714 \* indicates  $P < 0.05$ , \*\* indicates  $P < 0.01$ .